Clumped isotope analysis of central Australian carbonates: A potential palaeoclimate proxy for Australia's arid interior

Thesis submitted in accordance with the requirements of the University of Adelaide for an Honours Degree in Environmental Geoscience

Fletcher Clancy Nixon

November 2021

Word Count: 7996

THE UNIVERSITY of ADELAIDE

TITLE

Clumped isotope analysis of central Australian carbonates: A potential palaeoclimate proxy for Australia's arid interior

RUNNING TITLE

Clumped isotope palaeotemperatures for Australia's arid interior

ABSTRACT

Quantitative records of past temperature variability in arid environments are crucial for validating climate models and their ability to capture the full range of the Earth's surface. However, arid region temperature reconstructions are rare, particularly in the Southern Hemisphere, including Australia. The recently developed clumped isotope thermometer provides a novel approach to potentially address this demand by allowing the estimation of carbonate precipitation temperature independent of environmental water isotopic composition. Two types of carbonate materials offer potential for clumped isotope temperature reconstructions in arid central Australia: fossil mollusc shells deposited within the shoreline sediments of now dry lakes, and tufa deposits formed in springs fed by continuous discharge of Great Artesian Basin groundwater. Clumped isotope analysis was conducted for a suite of tufas from central Australian mound spring deposits in addition to a series of lake shells from the same region. Micro-XRF mapping was used to evaluate sample quality and heterogeneity, alongside XRD analysis. In addition to benefitting clumped isotope analyses, these data may improve the data quality and success of U-series dating of mound spring tufas. Air temperatures inferred from tufa Δ_{47} measurements suggested temperatures ~5°C cooler than modern-day conditions during the early Holocene, which supports previous palaeoclimate models for central Australia. Palaeotemperatures ~17°C cooler than present were inferred from shells during 70-35 ka, with two warmer periods coinciding with lake filling episodes during ~48 and ~33 ka. Carbonate $\delta^{18}O$ appeared largely to have been driven by changes in water $\delta^{18}O$ for lakes but not mound springs, reflecting different hydrological controls on the two water sources. Agreement between temperatures and palaeoclimate models suggest clumped isotope analysis may function as a valuable quantitative palaeotemperature proxy in central Australia. Analysis of additional tufa and shell samples should be prioritised, in addition to further studies into the genesis of different tufa.

KEYWORDS

Late Quaternary, carbonates, Central Australia, clumped isotopes, palaeoclimate, palaeotemperature

TABLE OF CONTENTS

LIST OF FIGURES AND TABLES

1. INTRODUCTION

Detailed palaeoclimate records are valuable for the development and validation of climate models, which have important consequences for predictions of future climate change. Efforts have been made to refine estimates of palaeoclimate changes through the Last Glacial Maximum (LGM) to better constrain climate sensitivity to changes in CO_2 and establish a reference point for climate models for future climate scenarios (Uemura *et al*., 2012; Fitzsimmons *et al*., 2013; Srivistava *et al*., 2015). Most palaeoclimate records worldwide are sourced from marine or near-marine proxies, with a scarcity of palaeoclimate data from semi-arid and arid environments and a distinct latitudinal bias to temperate or cooler climates in broader climate reconstructions

(Nanson *et al*., 2008; Reeves *et al*., 2013; Gilganic *et al*., 2014; Miller & Fogel, 2016). There is therefore a need for new temperature reconstructions from arid landscapes that span large scale shifts in the Earth system.

This is particularly a problem for Australia, where the extent and intensity of global climate cycles remains poorly defined during and prior to the LGM for approximately half of Australia's landmass (Fitzsimmons *et al*., 2013). Of particular interest are quantitative estimates of past air temperature, which remain poorly reconstructed for central Australia, despite their importance for climate modelling.

The recently developed 'clumped isotope' carbonate thermometer applied to calcium carbonates presents a potential solution to the need for quantitative palaeotemperature estimates in central Australia. The clumped isotope carbonate palaeothermometer exploits the correlation between mineralisation temperature and the frequency of bonding between ^{13}C and ^{18}O, due to the greater thermodynamic stability of the ^{13}C–^{18}O bond at lower temperatures (Ghosh *et al*., 2006; Eiler, 2007). Unlike palaeotemperature inferences using single element isotope geochemistry (e.g. $\delta^{18}O$) (Kim & O'Neil, 1997), clumped isotope estimations of mineralisation temperature are independent of environmental water isotopic compositions, which are often unknown in terrestrial settings for carbonates such as calcareous spring deposits, speleothems, and soil carbonates (Eiler *et al*., 2007; Spencer & Kim, 2015). Clumped isotope analysis also enables inferences of environmental water $\delta^{18}O$, which is valuable for reconstructing palaeohydrology (Eiler *et al*., 2007).

Calcareous spring deposits are widespread in central Australia, resulting from groundwater discharge from the Great Artesian Basin (GAB) (Keppel *et al*., 2011). Tufa samples have been collected and dated with U-series by Priestley *et al*. (2018), with the spring carbonate record extending back to ~500 ka. During this window, periods of coeval spring deposition have been interpreted to reflect periods of regionally high precipitation and groundwater discharge. To date, no clumped isotope analyses of mound spring tufas have been reported, which in turn raises several questions regarding the integrity of both the isotope geochemistry as well as geochronology of such deposits. Consequently, it is important to be able to characterise the nature of carbonate deposition alongside isotope geochemical analyses, including the identification of possible primary and secondary carbonate, as well as different discrete depositional units.

Palaeoshorelines of central Australian playa lakes are iconic archives of the central Australian hydrological record (Cohen *et al*., 2012; Fitzsimmons *et al*., 2013), providing the only direct proxy for previous water depths. Carbonate mollusc shells are also widespread in central Australian playa lake shorelines. A suite of mollusc shells from lakes Callabonna and Eyre previously been studied by Cohen *et al*. (2012, 2015, in prep.), with the organisms growing within these lakes dating back to 70 ka. Mollusc shells have previously been used for clumped isotope analysis (Henkes *et al*., 2013; Wang *et al*., 2016, 2021; Falster *et al*., 2019), although no clumped isotope studies have been conducted for central Australian lake shells.

This paper describes the application of clumped isotope analysis for a suite of previously dated central Australian tufas and lake molluscs to reconstruct central Australian palaeotemperature during the last ~340 ka. Micro-XRF mapping of tufa samples was used prior to clumped isotope analysis to screen for secondary carbonate precipitation or contamination, which could potentially affect U-series and clumped isotope data quality. These data will be used to test the hypothesis that palaeoclimate model simulations provide realistic estimates of cooler LGM temperatures and attempt to validate previous proxy temperature estimates for the region. The relationships between inferred temperature and $\delta^{18}O$ for source water and bulk carbonate will be tested and used to describe the environments in which carbonate precipitated. Due to the general dearth of palaeoclimate data from arid and semi-arid zones globally, this investigation provides an important case study towards increasing our understanding of climate change in desert regions worldwide.

2. BACKGROUND

2.1 Central Australian palaeoclimate

The Australian mainland is situated distally from primary glacial-interglacial amplifiers of climate change, such as ice sheet-albedo feedback effects. This, in conjunction with generally flat topography, means that the continent acts as a passive record for large-scale climate and should directly reflect global climate changes (Miller *et al*., 1997; Gimeno *et al*., 2010). Approximately half of Australia's landmass consists of arid or semi-arid environments (Figure 1), with the continental interior experiencing considerable climatic fluctuations during the Quaternary (Bolwer, 1976; Hesse *et al*., 2004; Gilganic *et al*., 2014). Within this region, reliable natural climate variability

records over glacial-interglacial timescales have been pursued for decades to provide a framework for better understanding the climate system in central Australia (Miller *et al*., 1997). However, despite increasing attention in recent years, these past climatic changes remain poorly defined in terms of both intensity and time (Hesse *et al*., 2004; Fitzsimmons *et al*., 2013). Complications pertaining to arid and semi-arid Australian palaeoclimate records generally relate to the poor preservation potential for organic matter, such as charcoal and pollen (Hesse *et al*., Gilganic *et al*., 2014). Consequently, most palaeoenvironmental reconstructions for the continental interior rely heavily on discontinuous and qualitative geomorphic archives with relatively large chronological uncertainties, such as dunes and playas, which presents obvious difficulties in quantifying palaeoclimate change in the region (Fitzsimmons *et al*., 2013; Treble *et al*., 2017).

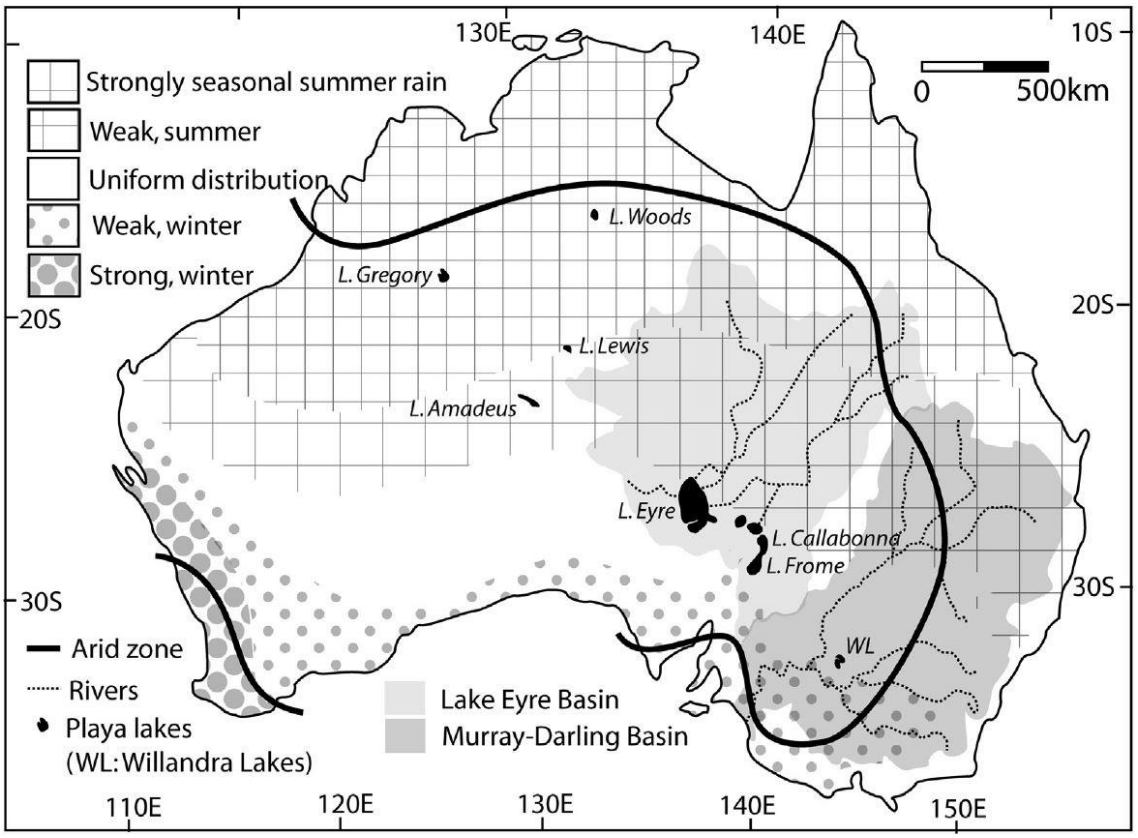

Figure 1: Map of the distribution of rainfall seasonality for the Australian mainland. The transition from semi-arid to arid climate is indicated by a thick black line, while major playa lakes are also indicated in black. The large catchments of the Lake Eyre Basin (LEB) and Murray-Darling Basin (MDB) are shown in grey, along with the associated major watercourses. Modified from Fitzsimmons *et al.* (2013).

Recent progress has been made into better understanding environmental change in central Australia, principally through the development of palaeoclimate proxies such as geochemical data from soil carbonates, eggshells, pollen, microbial lipids, and plant phytoliths (Pearson *et al*., 2001; Miller *et al*., 2005, 2016; Bray *et al*., 2012; Fitzsimmons *et al*., 2013), improvements in the density and accuracy of dates, and better integration of different palaeoclimate reconstruction techniques (Fitzsimmons *et al*., 2013). However, conflicting evidence persists for low-latitude cooling and hydrological change during the Last Glacial Maximum (LGM), and quantitative climate records beyond ~50 ka remain elusive (Miller *et al*., 1997; Gilganic *et al*., 2014; Treble *et al*., 2017).

Early LGM palaeotemperature estimates in Australia were largely restricted to mountainous regions due to their reliance on proxies such as snowline and treeline depressions and certain diagnostic periglacial features (Galloway, 1965; Singh & Geissler, 1985; Colhoun & Fitzsimmons, 1990). Unfortunately, these temperature reconstructions rely on assumptions about past precipitation, conflict strongly with sea surface temperature (SST) reconstructions, and cannot be applied for the low-elevation Australian interior (Miller *et al*., 1997; Treble *et al*., 2017).

The most notable proxy of central Australian palaeotemperature has been amino acid racemisation in emu eggshell fragments (Miller *et al*., 1997). The temperature-dependent rate changes in amino acid racemisation have been used to infer cooling of millennial-scale air temperatures by at least 9°C during 45-16 ka BP, relative to those after 16 ka BP, reflecting global-scale cooling processes during this period (Miller *et al*., 1997). Alternative estimates of central Australian climate changes can be estimated using climate model hindcasts, as synthesised in the PaleoView model (Fordham *et al*., 2017). However, the absence of local data prevents validation or the identification and correction of biases for these palaeoclimate models.

Palaeohydrological reconstructions in central Australia have proven more productive than palaeotemperature and in some cases may provide an indirect means of inferring past temperatures in the region (Treble *et al*., 2017). Carbonate deposition from springs in the western GAB appears to occur episodically across multiple locations, which has been used to infer regional palaeohydrological controls (Priestley *et al*., 2018). Periods of high rainfall have been inferred for the large GAB recharge zone during 515-415 ka, 390-350 ka, 350-320 ka, 285-240 ka, 195-175 ka, 160-150 ka, 110-100 ka, and the last 30 ka (Priestley *et al*., 2018). These periods of increased discharge are supported by periods of higher effective precipitation in central Australia, as inferred from speleothem growth (Ayliffe *et al*., 1998), pollen records (Kershaw, 1994), ostracod valves (De Deckker *et al*., 2011), increased fluvial activity (Nanson *et al*., 2008), higher lake shorelines (Cohen *et al*., 2012, 2015; May *et al*., 2015), and stable isotopes from avian eggshells (Miller & Fogel, 2016).

Stable isotope analysis of speleothem records from the Flinders Ranges, South Australia, suggest a relatively wet climate between 18.9-15.8 ka, with a rapid transition to arid conditions at 15.8 ka (Treble *et al*., 2017). This aridification is consistent with southward migration of Southern Hemisphere mid-latitude westerly winds (Denniston *et al*., 2013; Treble *et al*., 2017) and is supported by regional geomorphic evidence (English *et al*., 2001; Turney *et al*., 2004; Denniston *et al*., 2013). This shift in palaeoaridity coincides with the large shift in average air temperatures interpreted for the region (Miller *et al*., 1997; Treble *et al*., 2017).

Palaeoshorelines of ephemeral lakes have been used to reconstruct continental aridity and moisture source changes in central Australia and filling histories for Lakes Mega-Frome (the combination of Lakes Blanche, Callabonna, Frome, and Gregory) and Mega-Eyre extending back to ~105 ka (Cohen *et al*., 2012, 2015). Palaeoshoreline age distributions for Lake Mega-Frome suggest multiple filling episodes of variable magnitude through the last glacial cycle, with the oldest recorded filling episode at 96 ± 7 ka, supported by regional geomorphology and accelerated speleothem deposition at Naracoorte and Kangaroo Island (Ayliffe *et al*., 1998). Additional filling episodes occurred during 65 ± 2.6 ka and 50-40 ka, with the two mega-lake systems last connected during the latter period (Cohen *et al*., 2012).

Filling episodes are also interpreted during 33-31 ka, 17.6-15.8 ka, and 13.2 ± 0.8 ka (Cohen *et al*., 2012), supporting previous records of wet intervals punctuated by episodic arid conditions (De Deckker *et al*., 2011). Conflicting filling records between Lake Mega-Frome and Lake Mega-Eyre raise the prospect of different water sources for

the two mega-lakes, which may require further hydrological modelling to adequately explain. Further examination of active moisture sources by Cohen *et al*. (2012) suggested palaeolake filling and drying phases in central Australia were at least partially driven by shifts in Southern Ocean circulation and tropical moisture sources, with Southern hemisphere insolation a poor indicator of filling episodes.

2.2 Clumped isotopes

The carbonate clumped isotope thermometer is a novel technique for inferring palaeotemperature, which exploits the preferential binding of heavy carbon (^{13}C) and oxygen (^{18}O and ^{17}O) isotopes. Rare, heavy isotopes of oxygen and carbon tend to increasingly "clump" together within a single molecule at lower temperatures, due to the greater thermodynamic stability of the ^{13}C–^{18}O bond. (Ghosh *et al*., 2006; Eiler, 2007). Higher entropy with increasing temperature prevents this preferential bonding, resulting in more random distributions of heavy isotopes (Ghosh *et al*., 2006). Unlike the traditional stable oxygen isotope ($\delta^{18}O$) paleothermometer, carbonate clumped isotope thermometry (quantified as Δ_{47}) is independent of source water isotopic composition, enabling application for a broader range of carbonate deposits (Eiler, 2007).

As Δ_{47} cannot be directly measured within calcium carbonate matrices, samples are dissolved in phosphoric acid, with the produced CO_2 reflective of the carbonate isotopic signature and measured with high-precision analyses (Huntington *et al*., 2009). Δ_{47} is used to represent CO_2 clumped isotope composition, which is defined by Equation 1:

$$\Delta_{47} = \left[\left(\frac{R^{47}}{R^{47*}} - 1\right) - \left(\frac{R^{46}}{R^{46*}} - 1\right) - \left(\frac{R^{45}}{R^{45*}} - 1\right)\right] \times 1000 \qquad (Eq. 1)$$

where R^i is the actual abundance ratio of CO_2 with mass *i* relative to the mass 44 ($^{12}C^{16}O_2$) and R^{i*} reflects the expected ratio of mass *i* relative to mass 44 for a stochastic distribution, whereby heavy isotopes are randomly distributed (Eiler, 2007; Huntington *et al*., 2009).

Analytically measuring mass 47 CO_2 ($^{13}C^{18}O^{16}O$) is incredibly challenging and requires highly sensitive mass spectrometry and the development of sophisticated purification techniques (Kocken *et al*., 2019). Advancements in clumped isotope analytical methods have enabled the use of reduced sample sizes without loss in precision (Meckler *et al*., 2014; Muller *et al*., 2017). An absolute reference frame using carbonate standards (Dennis *et al*., 2011), pressure baseline corrections (Meckler *et al*., 2014), the use of new parameters (Brand *et al*., 2010; Daëron *et al*., 2016; Schauer *et al*., 2016), and optimisation of carbonate standards (Kocken *et al*., 2019) have also been invaluable developments for clumped isotope research.

Unfortunately, interlaboratory discrepancies persist for clumped isotope studies (Daëron *et al*., 2016; Kocken *et al*., 2019). The exact cause for these differences is unknown, although possible causes include differences in standardisation schemes (gas versus carbonate standards), phosphoric acid preparation, kinetic effects during carbonate precipitation, or different mass spectrometry methods (Kocken *et al*., 2019). The choice of parameters and data treatment processes is insufficient for explaining interlaboratory discrepancies (Petersen *et al*., 2019), although the likelihood of interlaboratory differences can be assessed by measuring identical sample material at each laboratory.

The InterCarb carbon dioxide equilibrium scale ("I-CDES") has also been developed by Beransconi *et al*. (2021) as a thermometer calibration for a broad range of sample types including tufas and travertines but may not be suitable for rapidly precipitating mollusc samples. The I-CDES calibration has been previously demonstrated to fit for naturally precipitating tufas and travertines with calcite, aragonite, and mixes of these two carbonate types, with the aragonite regression statistically similar to that of calcite samples. As yet, statistical agreement between dolomite and calcite regressions remains inconclusive (Anderson *et al*., 2021), although separate calibrations have been developed for dolomite samples (Bonifacie *et al*., 2017).

Clumped isotope studies are complicated by solid-state reordering of C–O bonds in carbonate minerals (Passey & Henkes, 2012), as small degrees of reordering can cause large errors in temperature estimates (Staudigel & Swart, 2016). Clumped isotope compositions appear highly susceptible to aragonite reordering for moderate heating scenarios, such as early diagenesis or heating during drilling (Staudigel & Swart, 2016; Chen *et al*., 2019; Guo *et al*., 2019). Typically, temperature offsets from aragonite reordering are less than would be expected for daily or seasonal-scale temperature variations in most surface waters, with trends able to be interpreted if offsets are shared by all data (Staudigel & Swart, 2016).

2.3 Mound spring carbonates

Calcium carbonate is commonly deposited at mound springs from the degassing of CO_2 from groundwater that is saturated or supersaturated with dissolved carbonate minerals (Crossey *et al*., 2006; Faccenna *et al*., 2008), as indicated by Equation 2:

$$Ca^{2+}{}_{(aq)} + 2HCO^{-}{}_{(aq)} \rightarrow CO_{2(g)} + H_2O + CaCO_3 \qquad (Eq. 2)$$

Degassing of the carbonate-rich groundwater is largely influenced by decreased fluid pressure, fluid flow turbidity, and biological activity (Chafetz & Folk, 1984). These calcareous freshwater deposits form over a broad range of climatic conditions and often have very restricted lateral extent (Ford & Pedley, 1996; Keppel *et al*., 2011).

Spring carbonates are often divided into two forms: travertines and tufas. Travertine generally refers to hydrothermal deposits, which invariably lack *in situ* animal and macrophyte remains, while tufa is usually applied to describe those formed near ambient conditions, which can include plant and invertebrate remains (Ford & Pedley, 1996; Hancock et al., 1999). Identification can be complicated by interlayering of tufa and travertine, such as where cooling in distal areas of thermal flow has enabled colonisation by macro- and microphytes (Ford & Pedley, 1996). The term 'mound spring carbonates' will be used to refer to either travertine or tufa deposits precipitated from groundwater springs.

Mound springs are widespread in central Australia, resulting from GAB groundwater discharge (Keppel *et al*., 2011; Priestley *et al*., 2018). The GAB is Australia's largest groundwater basin, spanning approximately 1.7 million km^2, with recharge predominantly from the Great Dividing Range and to a lesser extent from the GAB's northern, western, and south-western margins (Love *et al*., 2013), with recharge zones encompassing multiple climatic regions (Radke *et al*., 2000). Groundwater is discharged by the region's primary confined aquifer, frequently referred to as the J Aquifer, which outcrops along the GAB's western region (Love *et al*., 2013). Groundwater migration is

slow, with most J Aquifer water the product of Pleistocene and early Holocene recharge during periods of wetter climate than present (Torgersen *et al*., 1991, 1992; Mahara *et al*., 2009; Love *et al*., 2013).

The GAB's western margin receives annual rainfall of 130-230 mm/yr and mean relative humidity levels of approximately 40% (Love *et al*., 2013), along with monthly mean maximum temperatures of approximately 28.8°C. Discharged groundwater at active springs is undersaturated in calcite, with carbonate mainly deposited as plant or microbial tufa (Keppel *et al*., 2011). Tufa deposits can gradually migrate and coalesce into larger-scale tufa platforms that are preserved up to 25 m above modern-day ground surfaces (Figure 2) (Keppel *et al*., 2011).

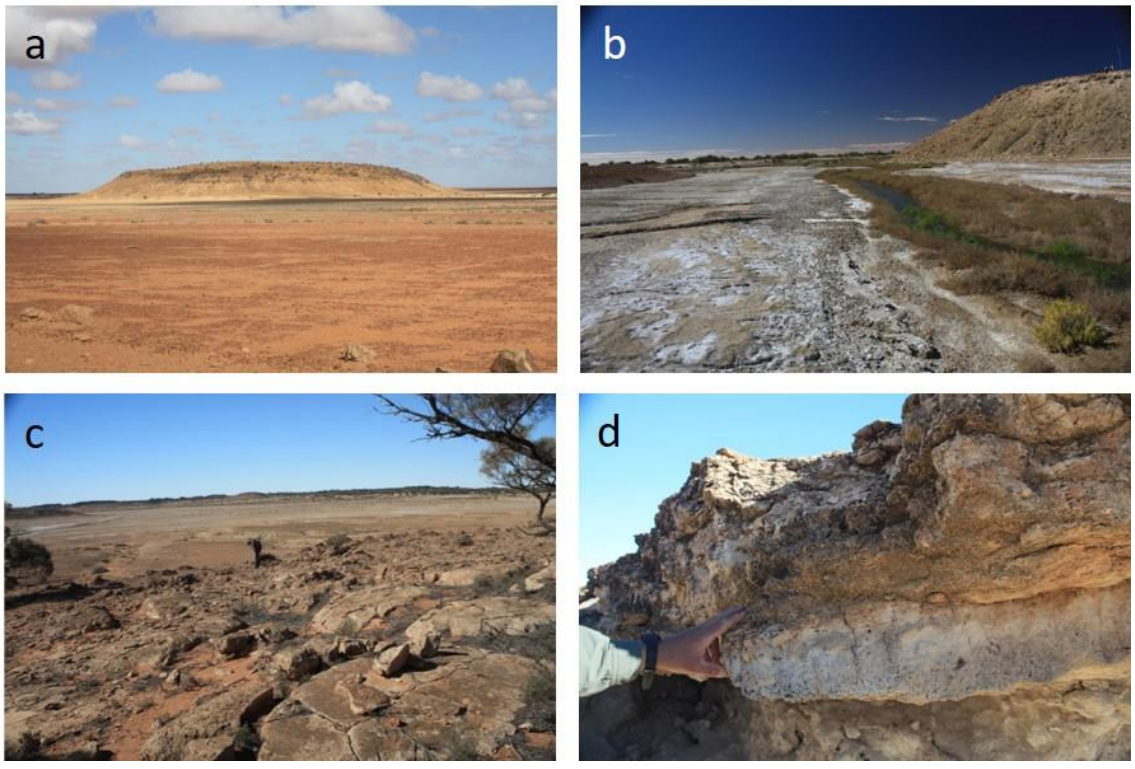

Figure 2: a) Beresford Hill mound spring site, consisting of a tufa platform capping a 45 m high hill. b) Dalhousie Springs actively flowing tail delta at the modern-day ground elevation. c) Tufa platform at Dalhousie Springs, currently situated 10 m above the current ground elevation. d) Banded feeder vein carbonate at Dalhousie Springs.

No seasonal variation in spring discharge has been observed for active springs, with groundwater insufficiently saturated in calcium carbonate to enable precipitation upon emergence (Keppel *et al*., 2011). An excess of CO_2 must be degassed before carbonate precipitation can occur, implying that surface waters are at ambient conditions when tufa precipitation occurs (Keppel *et al*., 2012). Tufa morphology suggests deposition in mostly shallow, sluggish waters with abundant microbial organisms and aquatic plants, which are important mediators for carbonate precipitation (Lu *et al*., 2000; Keppel *et al*., 2011).

A series of central Australian mound spring deposits were dated by Priestley *et al*. (2018) using U-series, which exploits the greater solubility of uranium in groundwater, relative to thorium, and the decay of uranium isotopes to daughter thorium isotopes within a closed system to determine carbonate material ages (Cheng *et al*., 2000; Mallick & Frank, 2002). Studied tufas were deposited episodically during the last ~500 ka, with coeval deposition across different locations indicative of regionally controlled spring discharge due to increased recharge and groundwater flow rates (Priestley *et al*., 2018). Some samples dated by U-series returned unrealistic U/Th isotope ratios consistent with open-system behaviour. These samples were excluded, raising concern about both the overall validity of chronologies and the success of future tufa dating, as well as the prospect that clumped isotopes could be undermine by diagenetic alteration and precipitation of secondary carbonates.

Traditional stable oxygen isotope thermometry cannot be applied for mound spring carbonates as source water $\delta^{18}O$ values are usually unknown, particularly due to spring

water evaporation (Kim & O'Neil, 1997; Kato *et al*., 2019). However, Δ_{47} thermometry can be applied on mound spring deposits, as it is independent of environmental water $\delta^{18}O$ (Ghosh *et al*., 2006; Eiler, 2007). Previous clumped isotope data collected from modern tufa and travertine samples demonstrate a strong correlation with temperature, while Δ_{47}-signatures appear to be independent of parent solution pH, mineralogy, and precipitation rate (Kele et al 2015; Kelson *et al*., 2017; Bernasconi *et al*., 2021). Importantly, no significant difference was observed between calcite and aragonite Δ_{47} values (Kele *et al*., 2015; Winkelstern *et al*., 2016; Guo *et al*., 2019).

2.4 Lake mollusc shells

As well as demarking the extent of ancient lakes, and thus past hydrology, lake palaeoshorelines preserve carbonate fossils, presenting an opportunity to apply Δ_{47} thermometry for past lake waters and infer past air temperatures. These data can be combined with the hydrological record to further unravel the interplay between past climate and hydrology in what is now an arid landscape. Mollusc samples for this study were taken from palaeoshorelines at Lakes Callabonna and Eyre, which have previously served as a proxy record of continental water balance, as described in Section 2.1.

The prosobranch gastropod genus *Coxiella* is abundant within palaeoshorelines of Lakes Callabonna and Eyre. The genus is endemic to Australia, although live specimens have not been recorded in either lake (Williams & Mellor, 1991). *Coxiella* ecology is poorly understood, although the duration for which ephemeral lakes hold water and inundation periodicity are likely important factors for their distributions (Williams & Mellor, 1991). Ephemerality has been suggested as the reason for *Coxiella's* modern-day absence from most of central Australia, although sub-fossil deposits indicate it was

once abundant (De Deckker & Last, 1988). *Coxiella* are not homogenously distributed throughout some lake bodies, with adults observed at depths above 6 m and juveniles at depths of up to ~25 m in Lake Bullenmerri, Victoria, which has been speculated to reflect downward migration of juveniles following reproduction in shallow regions (Timm, 1976). Different distributions for adults and juveniles are not apparent for all modern lakes, including the shallow and ephemeral Lake Tallinga, South Australia (Williams & Mellor, 1991). For most ephemeral lakes, *Coxiella* are more abundant near the shore, implying active movement and/or passive shell displacement (Williams & Mellor, 1991).

3. METHODS

3.1 Sample collection and dating

The tufa carbonates that were used for this study were collected from nine sample sites in the western GAB (Figure 3), with samples used for clumped isotope analysis sourced from Sulphuric Spring and Dalhousie Springs. Information for individual samples can be found in Appendix A. Samples were collected from both active and extinct mound spring deposits and platforms, and mostly sourced from primary mound barrage structures surrounding the spring vents (Figure 2) (Keppel *et al*., 2011). Tufa samples were collected during field campaigns in 2006 and 2009, which were dated previously by U-series at the Radiogenic Isotope Laboratory, University of New Mexico (for further details, refer to Priestley *et al*., 2018).

A suite of mollusc shells excavated from ancient shorelines from Lakes Eyre and Callabonna (during which Lake Callabonna was part of Lake Mega-Frome) were also

selected for this study (Figure 3). Mollusc samples are predominantly *Coxiella sp.*, with an unknown bivalve genus also studied (Appendix A). These samples were previously dated at the University of Wollongong through radiocarbon dating of shell carbonate and optically stimulated luminescence (OSL) and thermoluminescence (TL) dating of lake core sediments (for further details, refer to Cohen *et al*., 2012, in prep.).

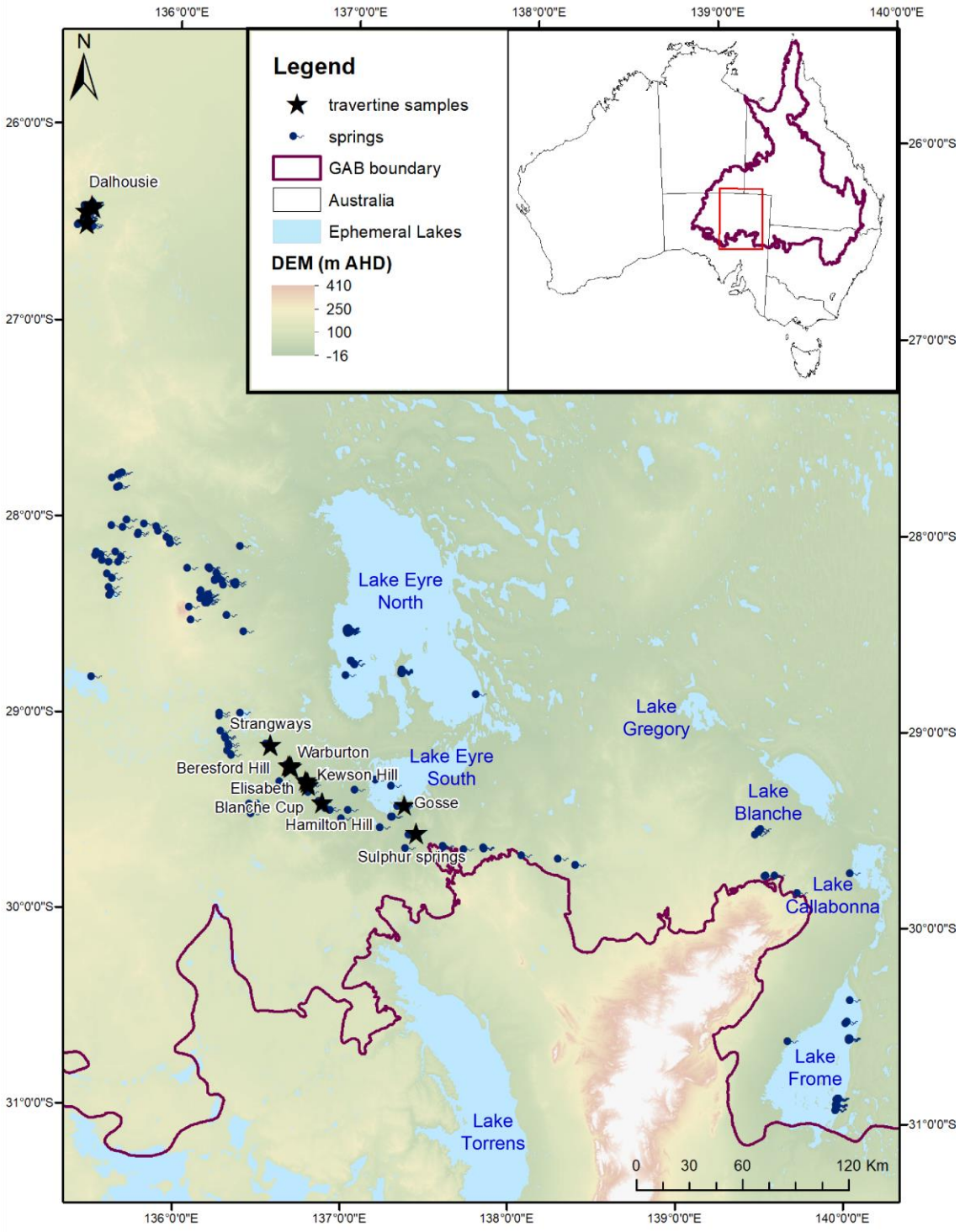

Figure 3: Map of central Australian sample locations in the western region of the Great Artesian Basin. Lake mollusc shell samples for this study were sourced from Lake Callabonna (Cohen *et al.*, 2012) and the southern portion of Lake Eyre North (Cohen *et al.*, in prep.).

3.2 Tufa microfacies analysis

High resolution chemical microfacies maps were made upon a subset of 25 previously dated tufa samples with the aim of validating U-series dating sites and to identify potential contamination within the spring carbonates. Of particular interest was the potential for establishing a correlation between U-series data quality and the concentrations of different elements within a sampled region. XRF analysis was conducted with a Bruker M4 Tornado micro-XRF spectrometer at Adelaide Microscopy, with XRF data collected from 75 µm sample spots and with a collection time of 35 µs per sample spot. The method for determining U-series quality can be found in Appendix B.

Semi-quantitative elemental concentrations were calculated for selected regions within XRF maps. The software used for quantification assumes selected areas are homogeneous and consists of one mineral phase. Hence, mineral inclusions were avoided where possible as they are not accounted for in the corrections used to calculate elemental concentrations. This method precludes the determination of mineral phases for elements that could occur both within the carbonate lattice (e.g. $FeCO_3$) and as inclusions from other minerals. Principal component analysis (PCA) and non-metric multidimensional scaling (NMDS) analysis were applied for statistical analysis of XRF data. Both PCA and NMDS were performed using the vegan package for R (Oksanen *et al.*, 2013).

X-ray diffraction (XRD) analysis was conducted in the Mawson Analytical Spectroscopy Services (MASS), University of Adelaide, to determine tufa mineralogy.

Samples were analysed using a Bruker D8 ADVANCE Powder X-ray Diffractometer with powders sprinkled on silicone wafers. XRD methodology is described further in Appendix B.

3.3 Sample preparation

Tufa samples were prepared for clumped isotope analysis using a dental drill to obtain ~50 mg of powder for each sample, sampling from the same layers as for U-series. Whilst aragonite concentrations within the tufas is believed to be low (Keppel *et al*., 2011), and the degree of Δ_{47} alteration due to reordering is likely to be small, drilling was conducted in intervals of less than ~15 seconds at a time interspersed by pauses in drilling of roughly equal duration to minimise heating and potential conversion of aragonite to calcite (Staudigel & Swart, 2016).

Mollusc shells were selected and manually cleaned with a fine brush and reverse osmosis (RO) water before treatment with pH 8 buffered 18% H_2O_2 solution for 30 minutes to remove any organic matter (Figure 4) (Falster *et al*., 2018; Roberts *et al*., 2018; Zhang *et al*., 2020). Treated shells were then rinsed four times with ultrapure 18 MΩ milli-Q water and oven-dried overnight at 40°C. Cleaned shells were finely ground into a homogenous powder with an agate mortar and pestle. Multiple individuals (n = 1 to 15) of a single taxon were combined to obtain sufficient powder for clumped isotope analysis, with the homogenous powders representing the average isotopic compositions for the shells within a sample layer.

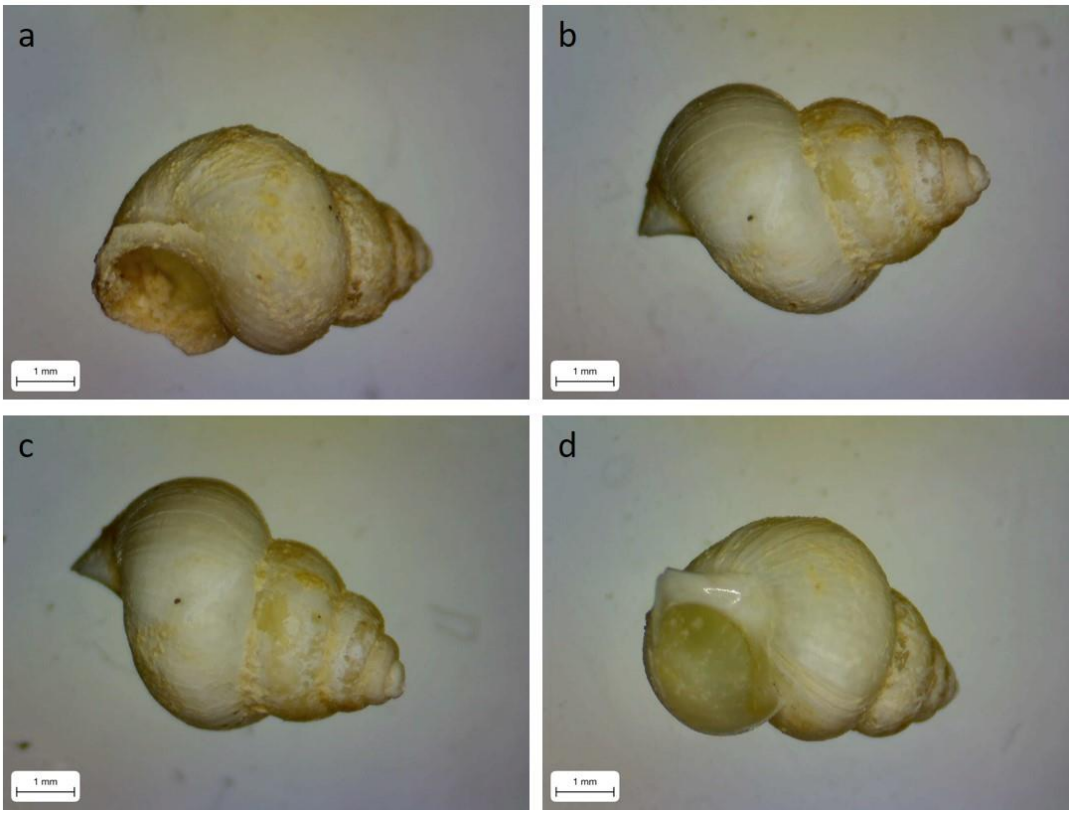

Figure 4: Effects of sample preparation process on individual lake shells after a) no treatment; b) manual cleaning; c) H_2O_2 treatment for 15 minutes; and d) H_2O_2 treatment for 30 minutes.

3.4 Clumped isotope analysis

Powdered samples were run for clumped isotope analysis with a Nu Instruments Perspective-IS stable isotope ratio mass spectrometer coupled to a Nu Carb sample preparation system at the University of Adelaide (UoA) and at the University of Melbourne (UoM), with identical sample preparation and methodology at both laboratories. Detailed analytical methods are provided in Appendix B. Briefly, ortho-phosphoric acid was introduced to powdered sample carbonate to produce CO_2 gas at a temperature of 70°C. This CO_2 gas was then purified through a Porapak^{TM} Q trap before a dual inlet mass spectrometer was used to measure Δ_{47}, $\delta^{13}C$, and $\delta^{18}O$ for purified sample gas relative to a working gas of known isotopic composition.

Raw sample Δ_{47}, were calculated using Equation 1, with R^i values were derived from the measured δ values for each isotopologue in the sample gas, relative to the working gas:

$$\delta^i = \left[\frac{R_{i\ (sample\ gas)}}{R_{i\ (working\ gas)}} - 1\right] \times 1000 \qquad (Eq. 3)$$

Uncertainty is reported as standard error:

$$\sigma_{\bar{x}} = \frac{\sigma}{\sqrt{n}} \qquad (Eq. 4)$$

where n is the number of replicates.

For both tufa and lake shell samples, 10 aliquots of 500 ± 25 µg carbonate samples were prepared and analysed. ETH standards 1-3 were used to correct data for pressure baseline (PBL) effects (Bernasconi *et al*., 2013; Meckler *et al*., 2014; Petersen *et al*., 2019) and to normalise raw Δ_{47} measurements into the absolute reference frame (Dennis *et al*., 2011) through a carbon dioxide equilibration scale (Daëron *et al*., 2021), with the I-CDES (Anderson *et al*., 2021; Bernasconi *et al*., 2021) scale used for tufas and CDES used for lake shells (Petersen *et al*., 2019). ETH-4 was excluded in favour of additional ETH-3 standards to increase sample Δ_{47} precision (Kocken *et al*., 2019). Conversion of raw measurements to the absolute reference frame was necessary to allow inter-laboratory comparison of results (Dennis *et al*., 2011; Bernasconi *et al*., 2018). An acid fractionation factor of +0.062‰ was used to adjust sample Δ_{47} values for the acid reaction temperature of 70 °C (Defliese *et al*., 2015).

The Δ_{47}, $\delta^{13}C$, and $\delta^{18}O$ values were calculated as the arithmetic mean average of the 10 aliquots for each sample, excluding any contaminated aliquots. All mollusc samples were analysed at the UoA, while all tufa samples used in this study were analysed at the UoM. Carbonate $\delta^{18}O$ and $\delta^{13}C$ values are reported relative to the Vienna Pee Dee belemnite standard (VPDB).

Once converted to the absolute reference frame, formation temperatures for each sample were calculated using the calibrations of Bernasconi *et al*. (2018) (Equation 5) for lake shells and Anderson *et al*. (2021) (Equation 6) for tufas:

$$\Delta_{47} = (0.0449 \pm 0.001) \times \frac{10^6}{T^2} + (0.167 \pm 0.01) \qquad (Eq. 5)$$

$$\Delta_{47} = (0.0391 \pm 0.0004) \times \frac{10^6}{T^2} + (0.154 \pm 0.004) \qquad (Eq. 6)$$

where *T* is the temperature in Kelvin for both calibrations.

In modern lakes, surface water temperature is consistently higher than mean annual air temperatures (MAAT). To correct for this effect in the palaeo-context, tufa and mollusc carbonate precipitation temperatures (T_{47}) were converted to MAAT using the transfer function of Hren & Sheldon (2012), which is independent of latitude, elevation, the size of the water body, and annual climatic conditions:

$$MAAT = -0.0318 \times T_{water}^2 + 2.195 \times T_{water} - 12.607 \qquad (\text{Eq. } 7)$$

where T_{water} is the mean annual water temperature and both *MAAT* and T_{water} are in °C ($R^2 = 0.96$).

Calcite-water oxygen isotope fractionation was calculated with the equation of Kim *et al.* (1997) using T_{47}:

$$1000\alpha_{calcite-water} = 18.03 \times \frac{10^3}{T_{\Delta_{47}}} - 32.42 \qquad (Eq. 8)$$

with environmental water $\delta^{18}O$ values then calculated for mineral formation:

$$\alpha_{calcite-water} = \frac{R_{calcite}}{R_{water}} \qquad (Eq. 9)$$

where *R* represents the ratio of ^{18}O to ^{16}O isotopes. $R_{calcite}$ is measured directly during clumped isotope measurements, enabling calculation of R_{water} and thus water $\delta^{18}O$. Environmental water $\delta^{18}O$ values are reported relative to Standard Mean Ocean Water (SMOW).

4. OBSERVATIONS AND RESULTS

4.1 Microfacies analysis

XRD analysis for the tufa samples revealed a complete absence of aragonite for all samples that were used for XRF mapping and/or clumped isotope analysis, except for those sampled from Sulphuric Spring (SUL 1a-f). Sulphuric Spring samples used for clumped isotope analysis consisted of ~15-70% aragonite, with the remaining portion composed of calcite (and trace concentrations of chalcopyrite for SUL 1a). Most samples consisted predominantly or entirely of calcite (including sample DAL 4C). Small traces of quartz were detected in most samples. Dolomite was detected in 6 out of the total 21 tufa samples for which XRD analysis was performed.

XRF mapping was conducted for 25 tufa samples (including all XRD samples), covering a broad range of depositional ages and palaeoenvironments. Different mineral

phases are identifiable for most samples (Appendix C), supporting the XRD results. Dolomite-bearing tufa samples feature > 5 wt.% magnesium, while aragonite-bearing samples from Sulphuric Spring (Figure 5) can largely be distinguished by > 3 wt.% strontium, compared to < 1 wt.% strontium in most other samples. All samples containing dolomite were poorly dated by U-series. Several different morphologies can be seen from the XRF maps, including laminated structures, lithic contaminants, and secondary precipitation of calcite or dolomite. Examples of the various tufa morphologies are shown in Figures 5-8, with further examples shown in Appendix C. Overall, reliably dated tufas were high in calcite or aragonite, with low amounts of lithic contaminants and magnesium.

Sample SUL 1 (Figure 5), for which clumped isotope analysis was conducted, demonstrated very small variation in calcium and low iron, magnesium, and silicon concentrations. Strontium and titanium concentrations are higher than for most other well-dated tufa samples. A hiatus in deposition can be inferred immediately before and after ~20 ka (layer a). Later deposition at the rate of ~0.5cm/kyr can be seen from ~12.3 to ~11.5, with another hiatus shown by a darker, strontium-rich layer. More recent carbonate precipitation was more rapid, with an average of ~2.7 cm/kyr during 9.7-9.3 ka. Carbonate for this period is more depleted in strontium than for older layers and becomes increasingly depleted in strontium after ~9.7 ka.

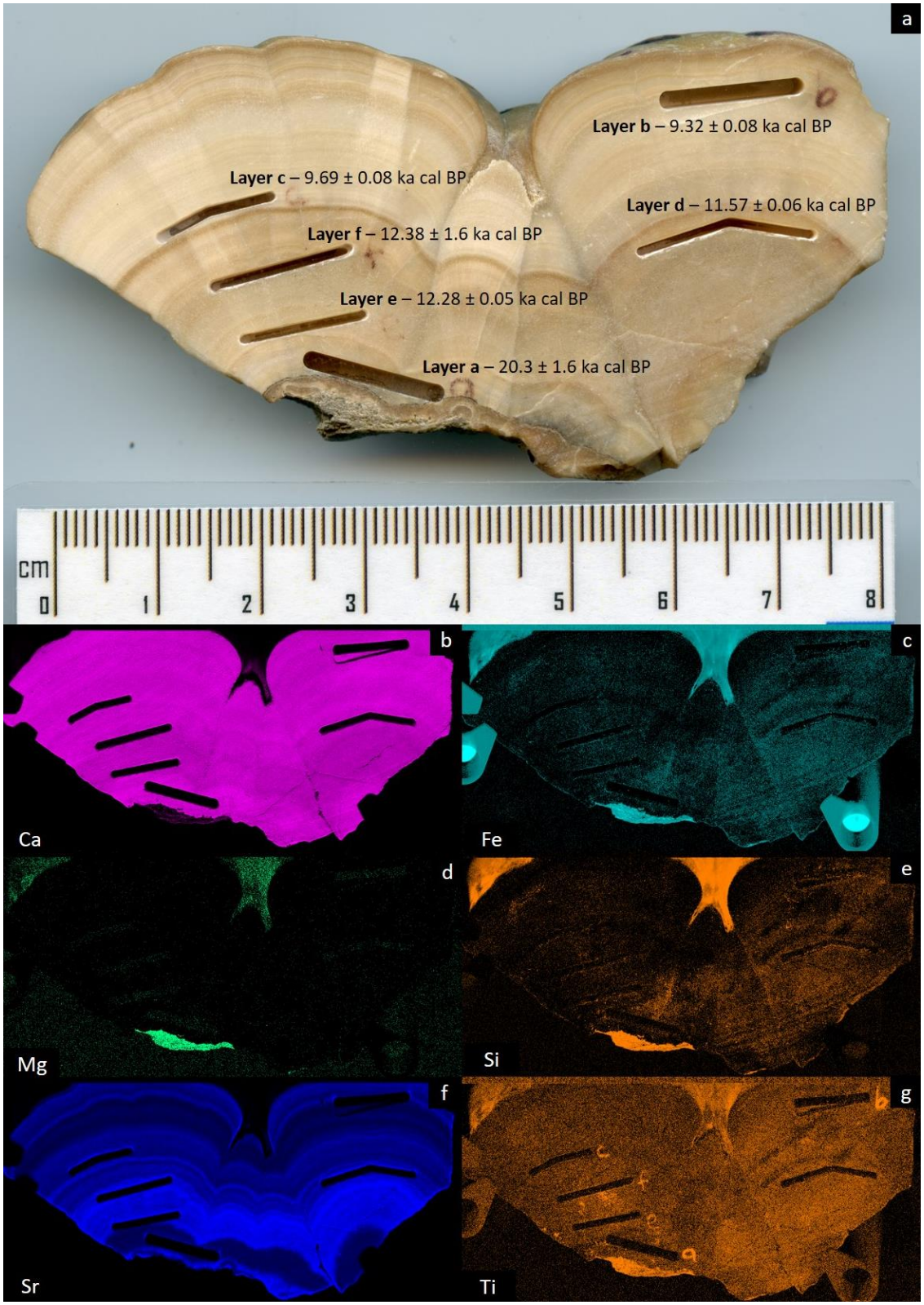

Figure 5: Tufa sample SUL 1 from Sulphuric Spring, showing a) sample layers and associated ages and XRF maps for b) calcium; c) iron; d) magnesium; e) silicon; f) strontium; and g) titanium.

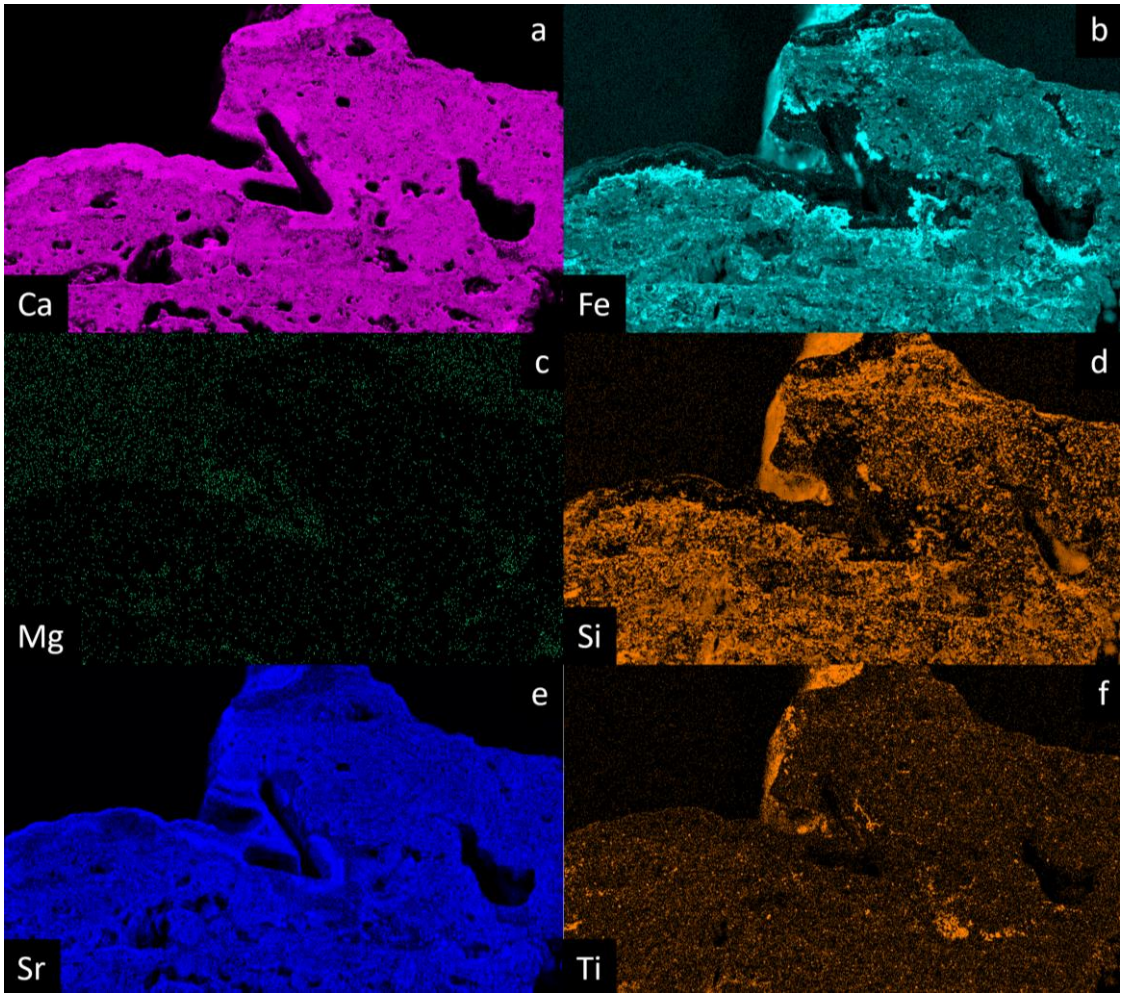

Figure 6: XRF map for well-dated tufa sample DAL 1A from Dalhousie Springs, showing a) calcium; b) iron; c) magnesium; d) silicon; e) strontium; and f) titanium. The bulk of the tufa is lithic-dominated, with relatively high abundances of silicon and iron.

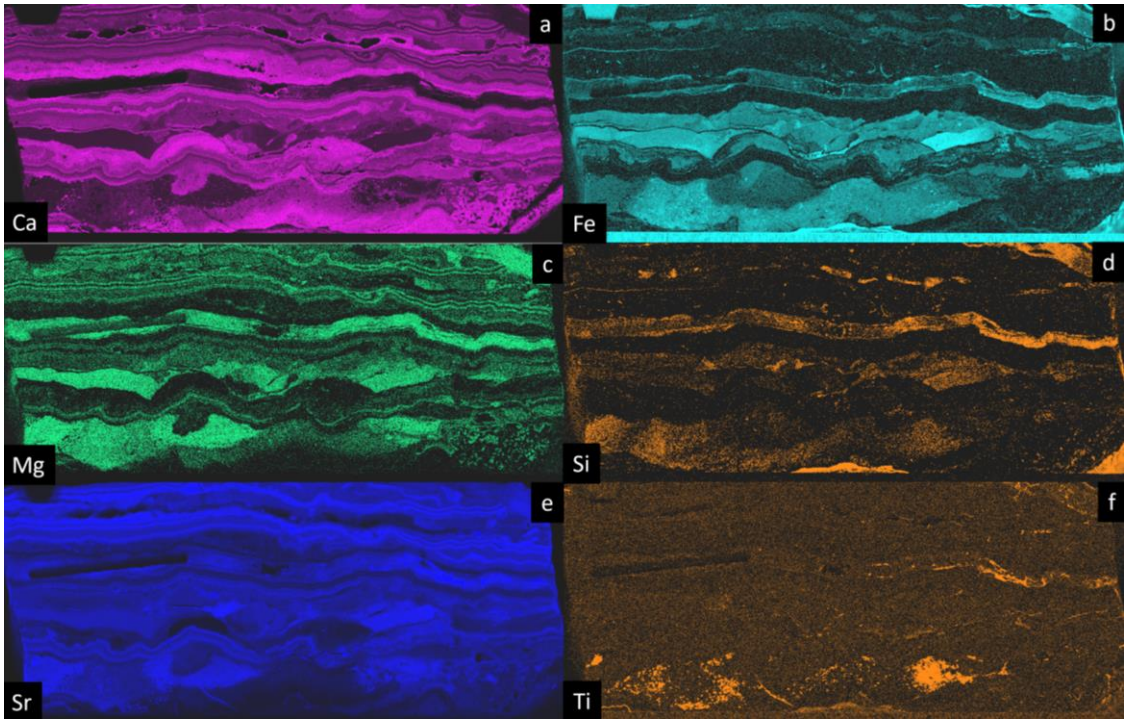

Figure 7: XRF map for poorly-dated tufa sample JER 3 from Jersey Spring, showing a) calcium; b) iron; c) magnesium; d) silicon; e) strontium; and f) titanium. Many of the layers are secondarily precipitated dolomite, including the dated sample layer, which features high magnesium, iron, silicon, and strontium, relative to the calcite layers.

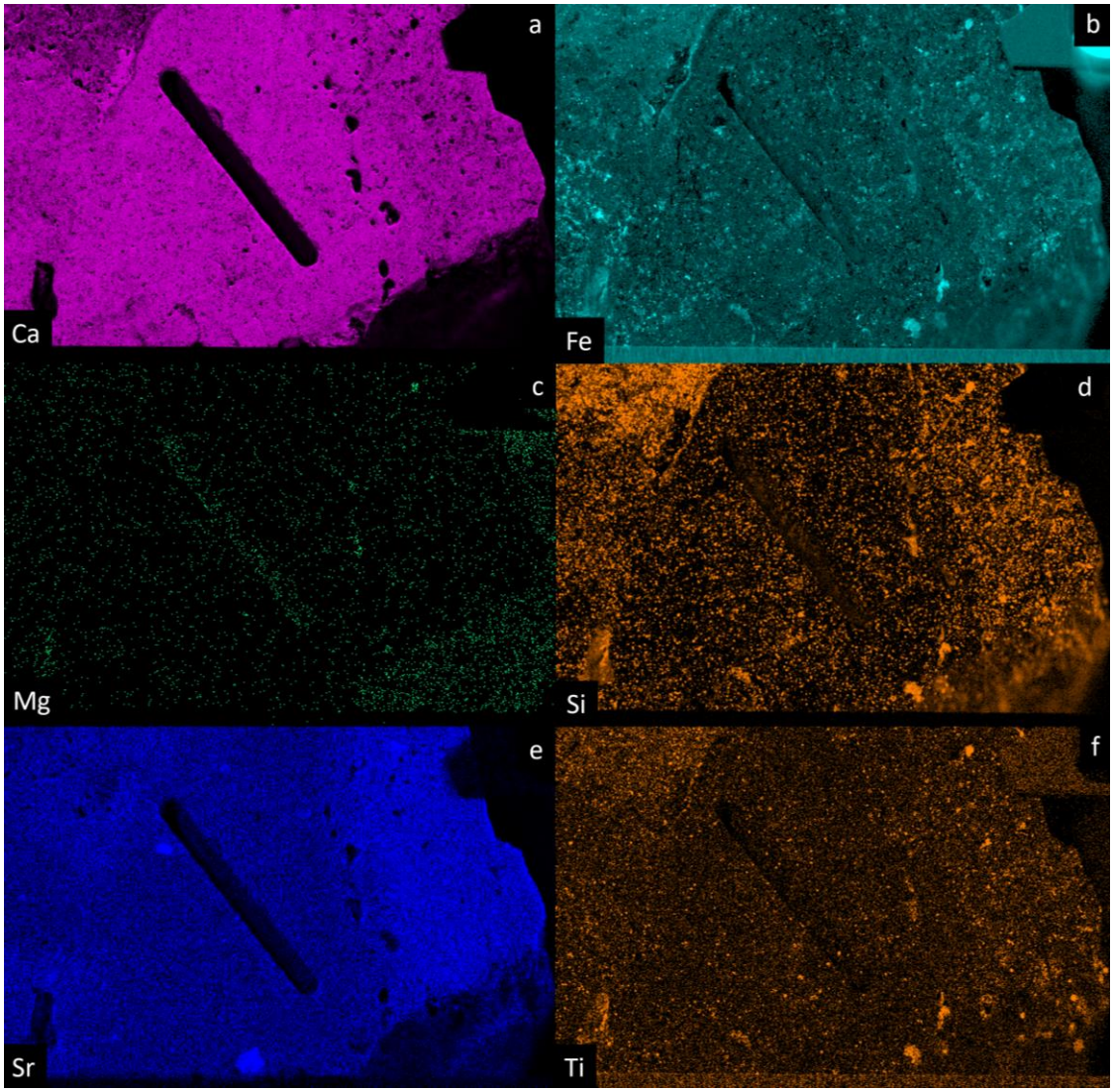

Figure 8: XRF map for poorly-dated tufa sample DAL 5 from Dalhousie Springs, showing a) calcium; b) iron; c) magnesium; d) silicon; e) strontium; and f) titanium. Small detrital grains can be seen in the tufa matrix, as indicated by high intensities of iron, silicon, and titanium, along with very low calcium concentrations. Dolomite is absent for this sample.

Semi-quantitative elemental abundances within sampled layers were calculated from micro-XRF, with 14 well-dated and 11 poorly-dated sample layers analysed (Appendix C). Elemental compositions of subsampled material were compared to previous estimates of the quality of U-series dates, with a view to better understanding sample selection for geochronology. PCA was conducted for tufa elemental concentrations (Figure 9) to better visualise variation within the multivariate dataset. Poorly-dated tufa

samples bearing dolomite differ significantly from other dated tufa samples in the PCA plots, while poorly-dated tufas without dolomite could not be completely differentiated by PCA, even when excluding dolomite-bearing samples (Figure 10). As with PCA, NMDS is only able to differentiate poorly-dated tufa samples for which dolomite is present (Appendix C).

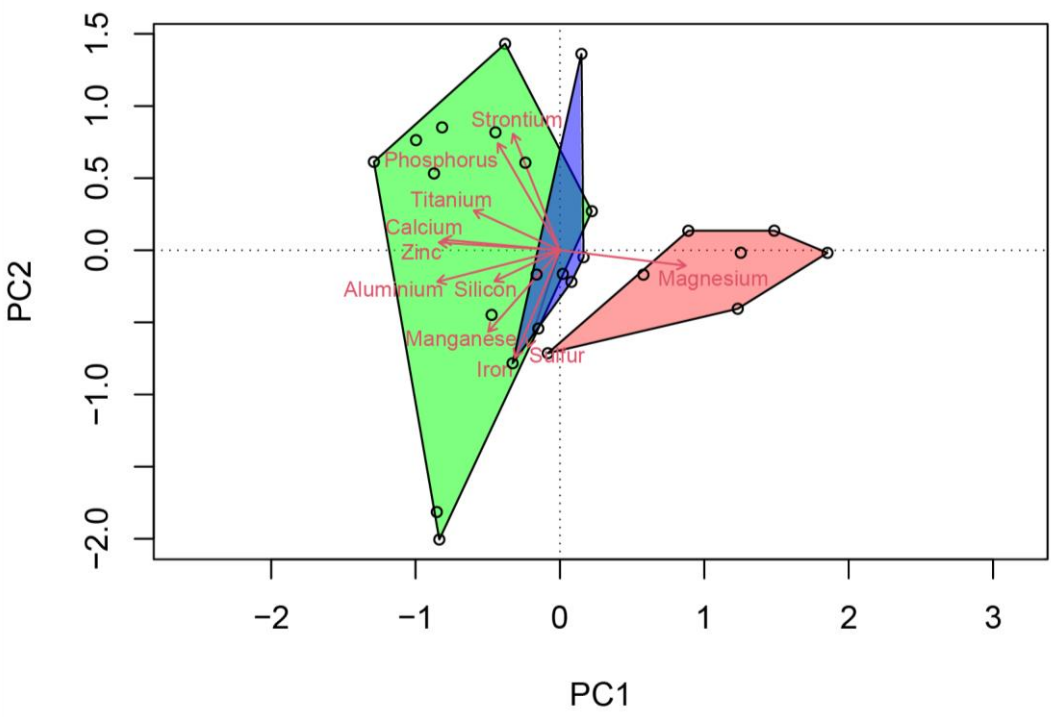

Figure 9: Principal component analysis for XRF data from central Australian mound spring tufas. Well-dated tufas are indicated by the green shading, with poorly-dated tufa samples separated in dolomite-bearing (red) and dolomite-absent (blue) subgroups.

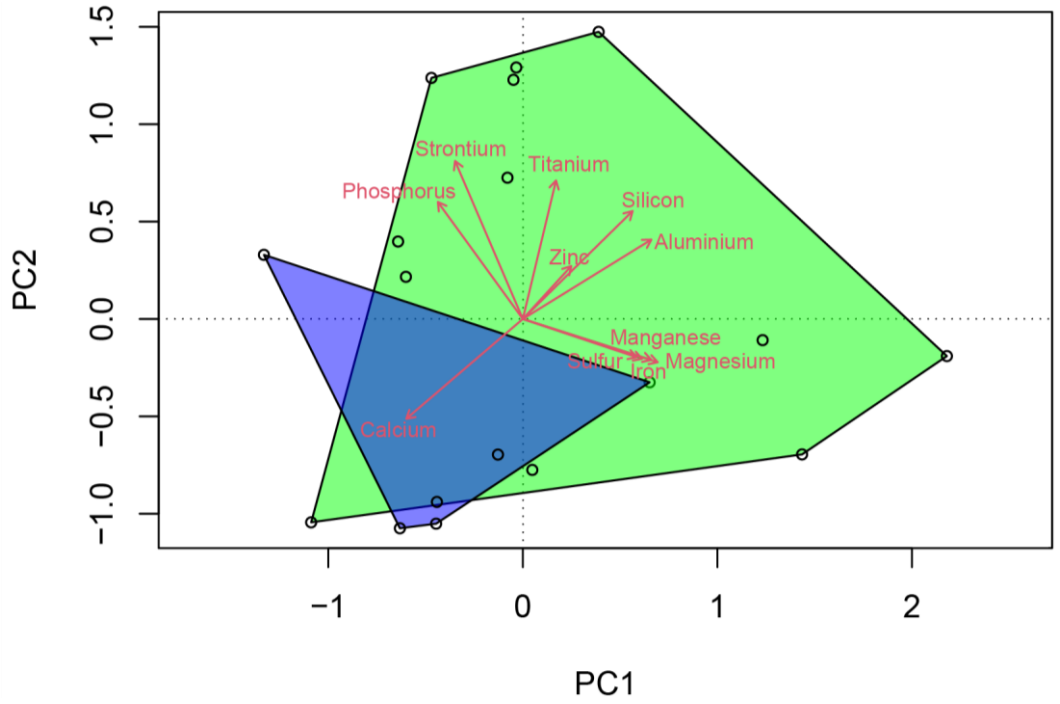

Figure 10: Principal component analysis for XRF data from central Australian mound spring tufas, with dolomite-bearing samples excluded. Well-dated tufas are indicated by the green shading, with poorly-dated tufa samples shown in blue.

4.2 Isotope data

Due to technical constraints, clumped isotope analysis could only be conducted for a restricted number of carbonate samples, with 7 tufas and 6 lake molluscs analysed. Sample material information, including locations, elevation, and shell counts for mollusc samples, can be found in Appendix A. Isotope data (Δ_{47}, $\delta^{18}O$, and $\delta^{13}C$) and estimated environmental water temperature and $\delta^{18}O$ values are summarised for tufas and lake shells in Table 1 and Table 2, respectively.

Table 1: Clumped isotope and stable isotope data for central Australian mound spring carbonates.

Sample ID	Sample Area	Corrected Age	$\delta^{13}C$	$\delta^{18}O$	Δ_{47} (corrected)	Error[a]	Estimated water temperature	Error[a]	$\delta^{18}O_{water}$	Error[a]
		ka cal BP	‰ VPDB	‰ VPDB	‰ (I-CDES)		°C		‰ SMOW	
SUL 1b	Sulphuric Spring	9.32 (0.08)	-2.24	-5.29	0.5342	0.0050	48.0	2.1	1.42	0.49
SUL 1c	Sulphuric Spring	9.69 (0.08)	-2.57	-5.61	0.5846	0.0048	28.5	1.7	-2.53	0.40
SUL 1d	Sulphuric Spring	11.57 (0.06)	-2.22	-5.93	0.5976	0.0049	24.0	1.7	-3.75	0.39
SUL 1e	Sulphuric Spring	12.28 (0.05)	-2.28	-6.04	0.5821	0.0048	29.4	1.7	-2.79	0.38
SUL 1f	Sulphuric Spring	12.38 (0.07)	-2.12	-6.31	0.5886	0.0051	27.1	1.8	-3.51	0.42
SUL 1a	Sulphuric Spring	20.3 (1.6)	-2.20	-5.10	0.5632	0.0048	36.3	1.8	-0.50	0.44
DAL 4C	Dalhousie Springs	334 (15)	-8.40	-6.08	0.6064	0.0051	21.1	1.7	-4.50	0.39

[a]errors reported as ±1 standard error (s.e.)

Table 2: Clumped isotope and stable isotope data for central Australian lake shells.

Sample ID	Sample Area	Corrected Age	$\delta^{13}C$	$\delta^{18}O$	Δ_{47} (corrected)	Error[a]	Estimated water temperature	Error[a]	$\delta^{18}O_{water}$	Error[a]
		ka cal BP	‰ VPDB	‰ VPDB	‰ (CDES)		°C		‰ SMOW	
LCP1 0.8	Lake Callabonna	33.4 (2.9)	0.14	2.37	0.7069	0.0076	15.2	2.0	2.72	0.46
LCP2 0.85	Lake Callabonna	39.6 (0.9)	-0.92	4.65	0.7123	0.0066	13.8	1.7	4.69	0.38
LCP1 0.96	Lake Callabonna	40.2 (1.0)	-4.02	0.93	0.7248	0.0116	10.6	2.9	0.25	0.65
CSP1 1.0	Lake Callabonna	48.4 (4.2)	0.29	3.08	0.7050	0.0065	15.7	1.7	3.54	0.36
CSP1 1.05	Lake Callabonna	51 (1.5)	0.31	3.61	0.7140	0.0088	13.4	2.3	3.55	0.53
WPLE P4B	Lake Eyre	70.8 (2.8)	-0.60	1.96	0.7193	0.0117	12.0	3.0	1.60	0.65

[a]errors reported as ±1 standard error (s.e.)

4.2.1 Stable isotope compositions

Tufa $\delta^{18}O$ values range from –6.31‰ (~12.38 ka) to –5.10‰ (VPDB) (~20.3 ka), whilst $\delta^{13}C$ values range from –2.57‰ to –2.12‰ (VPDB) for Sulphuric Spring samples with a single $\delta^{13}C$ value of –8.40‰ for Dalhousie Springs (Table 1). Lake shell $\delta^{18}O$ ($\delta^{18}O_c$) values vary from +0.93‰ to +4.65‰ (VPDB), whilst $\delta^{13}C$ values range from –4.02 to +0.31‰ (VPDB) (Table 2). Environmental water $\delta^{18}O$ ($\delta^{18}O_w$) values calculated from estimated water temperature range from –4.50 ± 0.39‰ to +1.42 ± 0.49‰ (SMOW) for tufas and from –0.25 ± 0.65‰ to +4.69 ± 0.38‰ (SMOW) for lake shell samples.

For tufas, no statistical correlation ($p > 0.05$) was observed between $\delta^{18}O_c$ and either $\delta^{13}C$ or T_{47}, whilst $\delta^{18}O_w$ correlates with T_{47} ($p < 0.05$, $R^2 = 0.9777$) and with $\delta^{18}O_c$ ($p < 0.05$, $R^2 = 0.7049$) (Figure 11). By contrast, for lake shells, no statistical correlation was observed between $\delta^{18}O_w$ and T_{47} ($P > 0.005$), while $\delta^{18}O_c$ correlates with $\delta^{18}O_w$ ($p < 0.05$, $R^2 = 0.9495$) (Figure 12). As with the tufa samples, no statistical correlation was observed between $\delta^{18}O_c$ and either $\delta^{13}C$ or T_{47}.

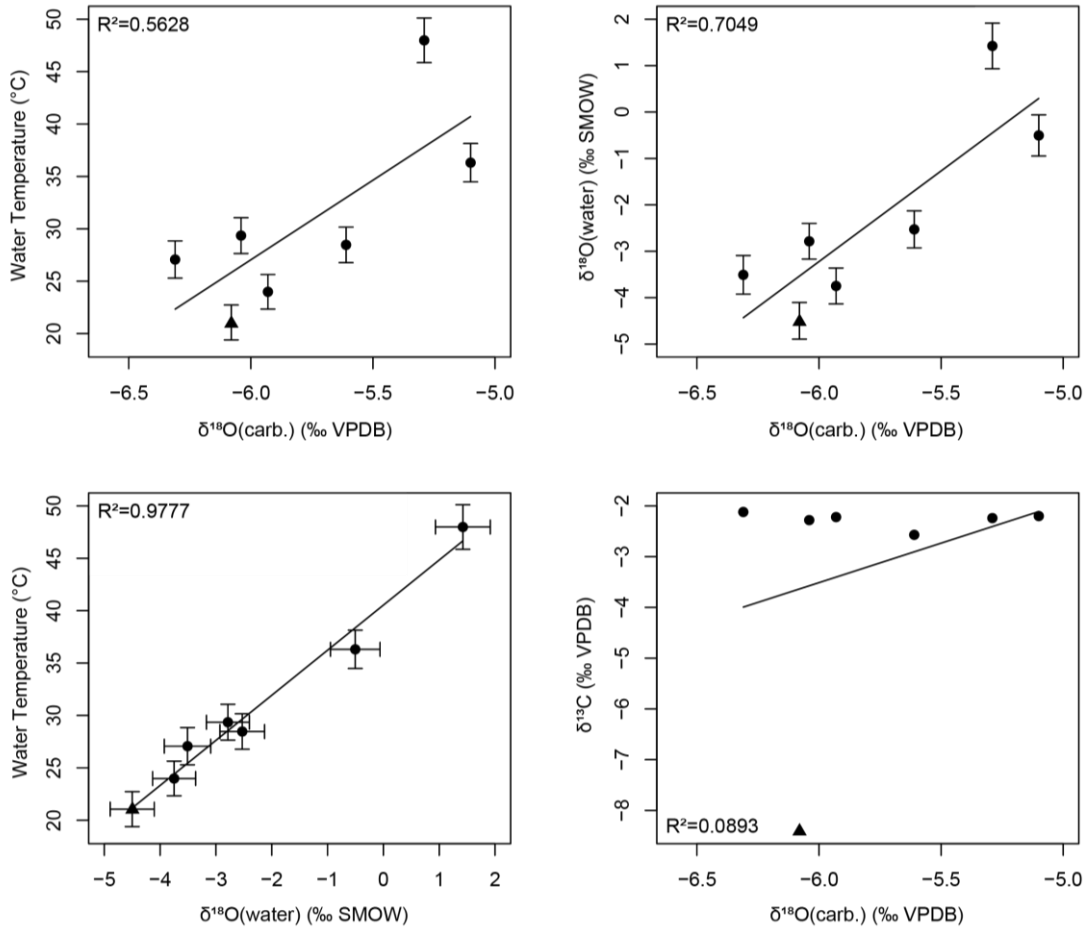

Figure 11: Relationship between isotopic compositions and temperature estimates from clumped isotope analyses on central Australian tufas. Sulphuric Spring samples are indicated by filled circles, with the Dalhousie Springs sample (DAL 4C) is indicated by a triangle symbol.

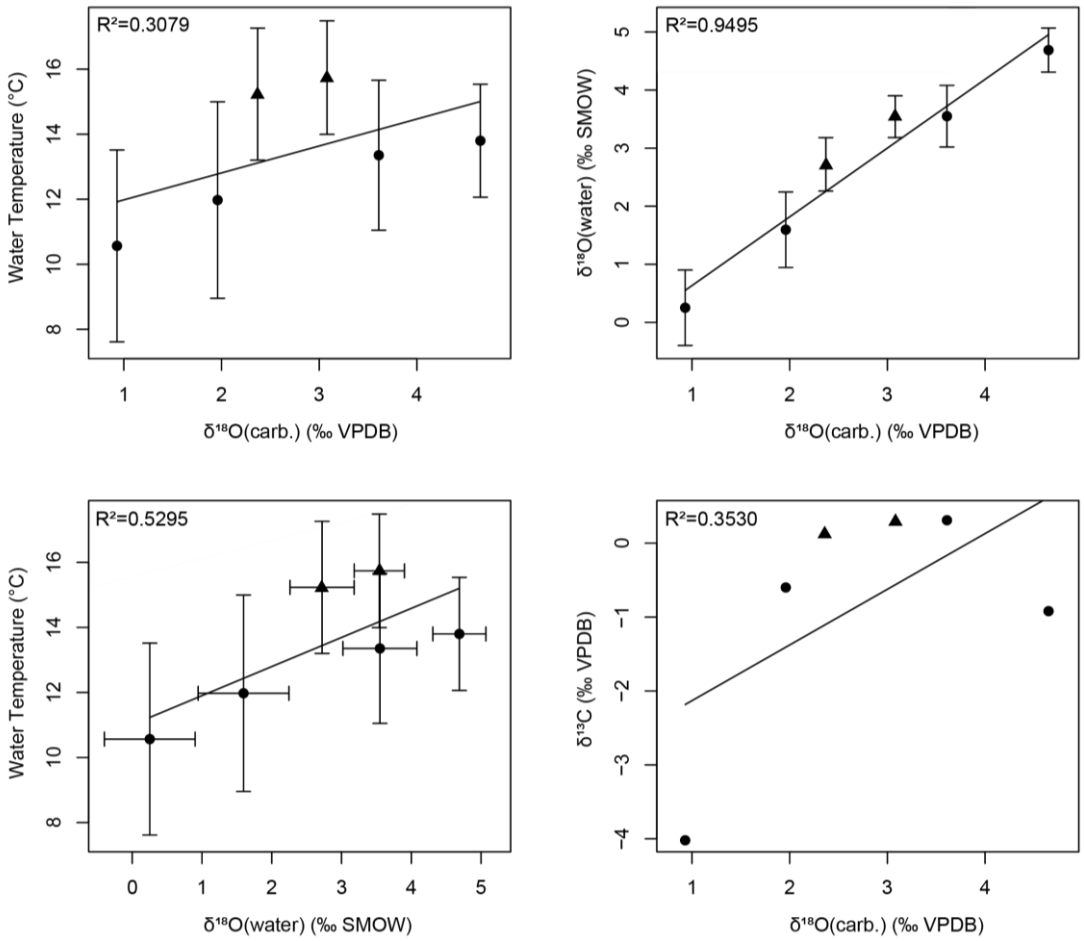

Figure 12: Relationship between isotopic compositions and temperature estimates from clumped isotope analyses on central Australian lake shells. Lake shells from lake filling episodes are indicated by triangle symbols, as interpreted by Cohen *et al.* (2012).

4.2.2 Clumped isotope compositions

Tufa Δ_{47} values range from 0.5342 ± 0.0050‰ to 0.6064 ± 0.0051‰ (I-CDES). For Sulphuric Spring, two of the six water temperature estimates (T_{47}) are notably high (36.3 ± 1.8°C at ~20.3 and 48.0 ± 2.1°C at ~9.32 ka), whereas the remaining four water temperature values range from 24.0 ± 1.7°C to ± 29.4 ± 1.7°C. These four samples suggest relatively consistent water temperatures of ~28°C, and MAAT estimates of ~24°C during 12.4-9.7 ka (Table 3). Δ_{47} values were compared to Sr/Ca, with the two anomalous samples coinciding with the lowest Sr/Ca. However, Δ_{47} (and thus, T_{47}) does

not appear to correlate with Sr/Ca (Figure 13). The single Dalhousie Springs sample suggests a water temperature of 21.1 ± 1.7°C and MAAT of 19.5 ± 1.9°C for ~334 ka.

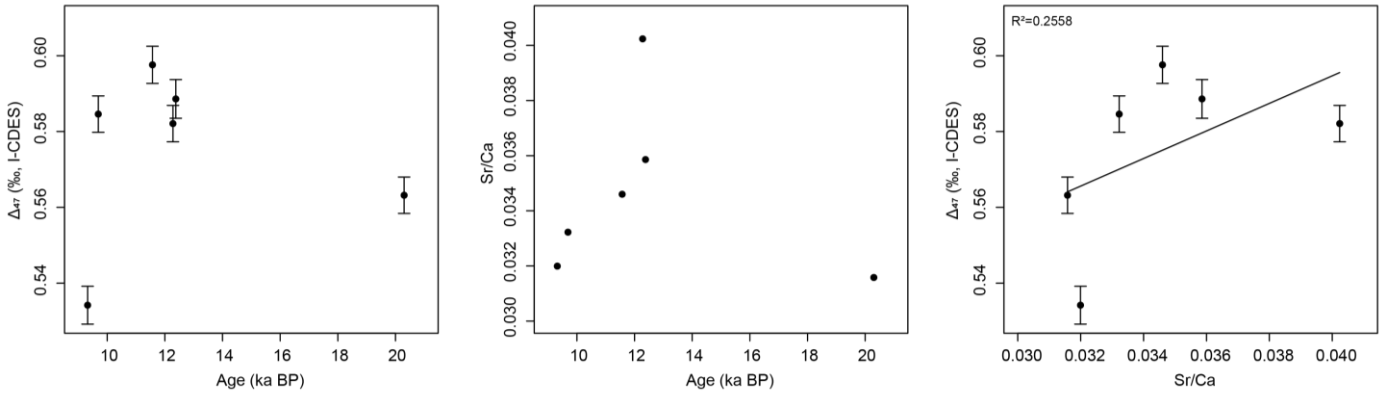

Figure 13: Sulphuric Spring tufa Δ_{47} and Sr/Ca records.

Lake shell Δ_{47} values range from 0.7069 ± 0.0076‰ to 0.7248 ± 0.0116‰ (CDES), with T_{47} between 10.6 ± 2.9°C and 15.7 ± 1.7°C during 51-33 ka. Water temperature of 12.0 ± 3.0°C was inferred for Lake Eyre (~71 ka), with most Lake Callabonna T_{47} values within this range throughout 51-40 ka (Table 1). Estimated MAAT values range from 7.0 ± 4.6°C to 14.1 ± 2.0°C for Lake Callabonna, with a single Lake Eyre MAAT of 9.1 ± 4.1°C at ~71 ka (Table 3).

Table 3: Clumped isotope and stable isotope data for central Australian carbonate samples.

Sample ID	Sample Area	Corrected Age	Estimated water temperature	Error[a]	MAAT	Error[a]
		ka cal BP	°C		°C	
SUL 1b	Sulphuric Spring	9.32 (0.08)	48.0	2.1	19.5	5.5
SUL 1c	Sulphuric Spring	9.69 (0.08)	28.5	1.7	24.1	2.1
SUL 1d	Sulphuric Spring	11.57 (0.06)	24.0	1.7	21.7	1.9
SUL 1e	Sulphuric Spring	12.28 (0.05)	29.4	1.7	24.4	2.1
SUL 1f	Sulphuric Spring	12.38 (0.07)	27.1	1.8	23.5	2.1
SUL 1a	Sulphuric Spring	20.3 (1.6)	36.3	1.8	25.2	2.7
LCP1 0.8	Lake Callabonna	33.4 (2.9)	15.2	2.0	13.4	2.4
LCP2 0.85	Lake Callabonna	39.6 (0.9)	13.8	1.7	11.6	2.1
LCP1 0.96	Lake Callabonna	40.2 (1.0)	10.6	2.9	7.0	4.6

CSP1 1.0	Lake Callabonna	48.4 (4.2)	15.7	1.7	14.1	2.0
CSP1 1.05	Lake Callabonna	51 (1.5)	13.4	2.3	11.0	2.9
WPLE P4B	Lake Eyre	70.8 (2.8)	12.0	3.0	9.1	4.1
DAL 4C	Dalhousie Springs	334 (15)	21.1	1.7	19.5	1.9

[a]errors reported as ±1 standard error (s.e.)

5. DISCUSSION

5.1 Microfacies analysis of tufa samples

Clumped isotope analysis of U-series dated mound spring tufas offers tremendous potential to develop quantitative climate records built on absolute chronologies. However, to have confidence in either the isotope analysis or the dating, it is necessary to screen the samples for contaminants, and to understand the potential for secondary alteration and remineralisation of the carbonate. To this end, micro-XRF mapping provides a valuable means of screening tufa samples to assess the validity of samples for past and subsequent geochemical analyses.

Micro-XRF mapping reveals several different tufa mineralogies, which are interpreted as largely reflective of different modes of deposition and varying lithic contamination. Tufas generally feature layered textures with lithic contaminants concentrated in discrete regions, suggesting variable amounts of dust entering the springs. Changes in deposition rate for Figure 5 are reflective of varying groundwater discharge rate, with strontium abundance lower for periods of greater carbonate precipitation rate. The presence of elements associated with detrital grains, such as aluminium, iron, and titanium, do not appear to negatively influence dating quality, contrary to the hypothesis of Priestley *et al*. (2018).

Micro-XRF scanning and associated XRD analyses indicated that several of the samples previously used for U-series dating contained dolomite, rather than the intended calcite or aragonite. These dolomite-bearing tufa samples, characterised by higher magnesium concentrations, appear to correspond with U-series dates that had been previously classified as unreliable (Priestley *et al*., 2018). Dolomite-bearing tufa samples differ significantly in XRF from samples for which dolomite is absent, suggesting that XRF scanning may serve as a potential tool for assessing sample quality prior to future U-series dating of mound spring carbonates. Dolomite may correspond to poor ages due to secondary, and therefore younger, dolomite precipitation overprinting or replacing the original carbonate (Figure 7). Poorly dated samples lacking dolomite (Figure 8) may result from fluid mobilisation and secondary alteration or remineralisation of carbonate resulting in open-system behaviour within tufa.

Whilst PCA and NMDS could not completely differentiate tufas with differing U-series date qualities, clustering of most poorly-dated samples suggests some elemental concentrations may be used to increase the probability of success for U-series ages. High magnesium carbonates should be avoided, with Mg/Ca ratios below 0.05 appearing to provide a reliable age for the tufas analysed in this study.

5.2 Tufa clumped isotope data

The data produced in this paper represents the first attempt to use clumped isotope analysis from central Australian mound spring carbonates to infer past water and air temperatures. Sulphuric Spring MAAT values inferred from T_{47} are realistic and within error of PaleoView (Figure 14), except for two outliers (discussed below). MAAT values are also within error of air temperatures predicted by previous central Australian

palaeotemperature studies (Miller *et al*., 1997; Treble *et al*., 2017). This suggests that clumped isotopes for tufas are a viable proxy for central Australian MAAT, which may be utilised for verifying palaeoclimate models and should continue to be explored as a novel proxy for palaeotemperature. This also supports the use of PaleoView for exploring ecological responses to palaeoclimate, at least for the early Holocene.

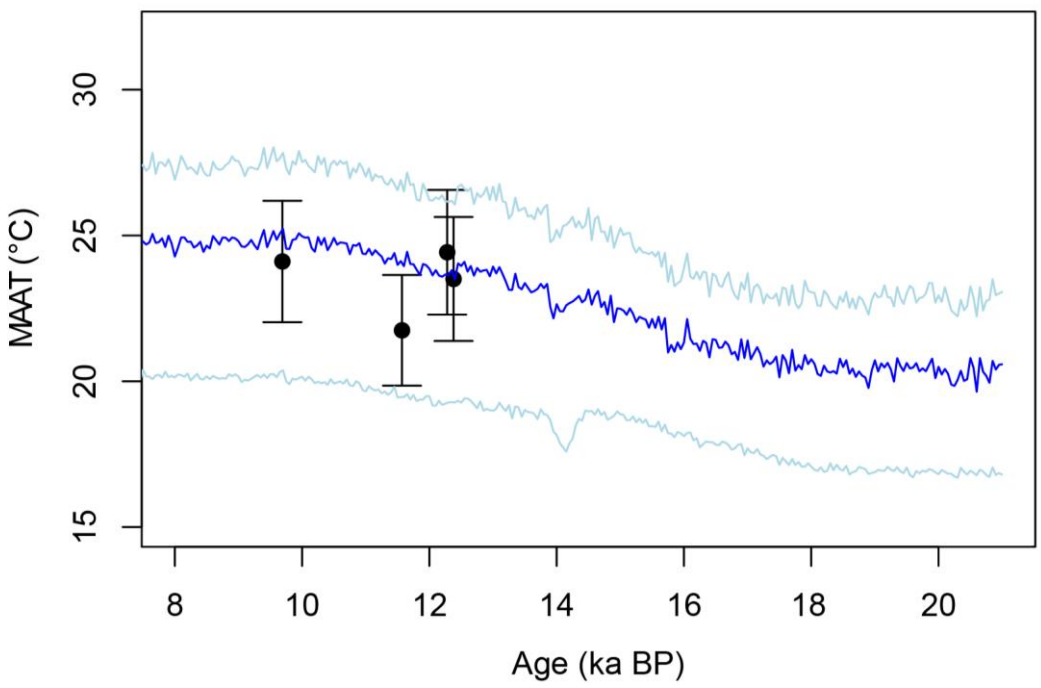

Figure 14: Comparison of central Australian tufa clumped isotope mean annual air temperatures (black circles) with modelled central Australian temperatures, as reconstructed by PaleoView (ver. 1.5.1) (blue line). The light blue lines indicate ± 1 s.e. uncertainty for the PaleoView model.

Several potential explanations can be put forward to explain the two tufa samples with anomalously high T_{47}, including aragonite reordering, tufa precipitation in disequilibrium with spring water, and hydrothermal heating. XRD implies that the outlier samples have sufficient aragonite concentrations to facilitate reordering of such magnitude (> 25% conversion of aragonite to calcite), although drilling duration should have been insufficient to enable reordering (Staudigel & Swart, 2016). Additionally, the characteristic decrease in $\delta^{18}O_c$ values (typically > 0.5‰) common to previous

experiments on aragonite reordering (Staudigel & Swart, 2016; Guo *et al*., 2019) is absent when comparing $\delta^{18}O_c$ with previous analyses (Appendix D).

Whilst the two outliers show distinctly low strontium concentrations, Sr/Ca does not appear to correlate with Δ_{47} (Figure 13), implying that Sr/Ca is not a clear indicator of aragonite reordering. It is possible that Δ_{47} variability for all tufa samples is due to variable aragonite reordering, with the tufas representing varying degrees of either contamination or alteration. The poor correlation of Sr/Ca and Δ_{47} seems to refute this, although it cannot be completely discounted without knowing initial Sr/Ca prior to possible reordering. Thus, aragonite reordering cannot be discounted as a cause of elevated T_{47}, either from drilling or occurring naturally prior to sampling.

Carbonate precipitation in disequilibrium with spring water is another possible explanation for the two outliers, supported by higher precipitation rates for sample SUL 1b (Figure 5). Recent studies have explored simultaneously obtained Δ_{47} and Δ_{48} values to identify and quantify biases in clumped isotope measurements due to reaction kinetics during carbonate precipitation (Fiebig *et al*., 2019; Bajnai *et al*., 2020). Unfortunately, the analytical method used in this study does not allow for the necessary high precision Δ_{48} values required to assess possible kinetic processes in the samples. Thus, the influence of precipitation kinetics cannot be determined from the obtained clumped isotope data.

Hydrothermally heating may also be a cause for the two outlying samples. However, this would require multiple tectonic shifts to allow for cooler (not hydrothermally

heated) waters between 12.4-9.7 ka and for modern Sulphuric Spring. Whilst multiple pauses in deposition and compositional changes can be seen within the tufa (Figure 5), this explanation is the least probable of the proposed causes for the two outlies.

At present, no clear best explanation can be put forward to explain the two anomalies, although aragonite reordering and reaction kinetics are the most probable causes. Data from the two tufa outliers will be excluded from subsequent interpretation.

Changes in deposition rates, flow rates, water depth, biological activity, geothermal heating, and the nature of the water body within the mound spring are potential causes for changes in tufa deposition or environmental water temperature (Kele *et al*., 2011, 2015; Kato *et al*., 2019). Unfortunately, these factors are difficult to reconstruct and microfacies analysis does not indicate any large shifts in depositional environment. The tufas have been assumed to have precipitated in equilibrium with environmental water, although disequilibrium could also explain unreliable Δ_{47} values (Fiebig *et al*., 2019). As discussed above, Δ_{48} precision is insufficient to detect kinetic effects in the tufa samples. Despite uncertainties regarding the nature of carbonate deposition and the water bodies in which the tufas precipitated, in addition to the rarity of surface water temperatures translating directly to air temperatures, inferred MAAT values should serve as a more suitable approximation of central Australian palaeotemperature T_{47}.

The single Dalhousie Springs sample (DAL 4C) represents the first surface palaeotemperature value obtained for central Australia during ~330 ka, with no previous quantitative data existing for comparison. Modern Dalhousie Springs waters are

geothermally heated, although it is unclear to what degree geothermal heating may have influenced T_{47} for DAL 4C, if any. During 334 ± 15 ka, benthic marine $\delta^{18}O$ was between 4-5‰ (SMOW), compared to 4.5-5‰ when the Sulphuric Spring tufa was deposited (Lisiecki & Raymo, 2005). The uncertainty for the Dalhousie sample age, puts the sample either within an interglacial or at the end of a glacial period terminating at ~337 ka (Lisiecki & Raymo, 2005). In the absence of additional samples for this period, caution is advised for the interpretation of this sample, although it appears that MAAT appears to have been ~4°C cooler for ~334 ka than when the Sulphuric Spring sample precipitated.

Mound spring $\delta^{18}O_w$ appears to be a more important driver of $\delta^{18}O_c$ than T_{47}, although the relationship between $\delta^{18}O_w$ and $\delta^{18}O_c$ is still relatively weak (Figure 11). T_{47} correlates strongly with $\delta^{18}O_w$, which is consistent with the expected relationship between $\delta^{18}O_w$ and evaporation. This also suggests that initial spring waters have relatively constant $\delta^{18}O$, which is supported by low $\delta^{18}O$ variability along groundwater flow paths (Radke *et al*., 2000). This is consistent with long residence times within the GAB (Love *et al*., 2013) and the hypothesis that spring $\delta^{18}O$ reflects the cumulative effects of the climate during groundwater recharge, mixing and possible fractionation during transport, and evaporation at the surface (Andrews, 2006). Consequently, conventional $\delta^{18}O_c$ analyses can be more confidently interpreted as a proxy for palaeo-evaporation, which appears strongly linked to water temperature. This may enable future high resolution tufa $\delta^{18}O_c$ analyses as a proxy for temperature-driven spring evaporation, which could serve as another novel proxy for central Australian palaeoclimate.

5.3 Mollusc clumped isotope data

Central Australian lake mollusc MAAT values suggest conditions during 70-33 ka that were ~15-22°C cooler than modern maximum temperatures in the region. MAAT values are supported by similar air temperature estimates (~11°C) during the same period, as inferred from eggshell amino acid racemisation (Miller *et al*., 1997). Two samples indicate relatively warmer conditions than other mollusc samples (~15°C), coinciding with lake filling episodes at ~33 ka and ~48 ka (Magee *et al*., 2004; Cohen *et al*., 2012, 2015).

As with tufas, lake shell MAAT assumes carbonate precipitation at the surface. However, geomorphic evidence suggests water depths of approximately 10 m prior to the LGM and ~15 m during filling episodes at 65 ± 2.6 ka and 50-40 ka, coinciding with overflowing of Lake Mega-Frome into Lake Eyre (Magee *et al*., 2004; Cohen *et al*., 2012, 2015). Most mollusc samples are *Coxiella* (5 out of 6 samples), which have been observed reproducing and growing in the upper 6 m of modern lakes despite lake depth, although this is challenged by some observed lake distributions (Timms, 1976; Williams & Mellor, 1991). Mollusc samples are assumed to have lived at similar depths despite varying lake volume, with T_{47} and MAAT trends reflecting regional palaeoclimate. Whilst temperature estimates may be lower due to carbonate precipitation at depth, this decrease is likely smaller than MAAT uncertainty (Haddout *et al*., 2018).

It should be emphasised that the mollusc T_{47} and MAAT estimates represent analyses of less than 15 individual shells per sample, with minimal shells favoured and one shell

used where possible (Appendix A). Consequently, shell data captures palaeoenvironmental conditions for the one-to-two-year windows during which the organisms were living. In the absence of detailed ecological studies, both *Coxiella* and bivalve samples are assumed to show similar seasonal cycles to modern permanent lakes. Hence, molluscs are assumed to grow mostly in spring, due to greater algal production and abundant food sources, with lake productivity generally decreasing in summer, due to depleted nutrients and excessive temperatures and light causing photoinhibition. It is entirely feasible that this was different for the LGM, but in the absence of any other data, this is assumed to be the case. If so, mollusc T_{47} values are possibly not dissimilar to mean annual temperatures, as modern spring temperatures are typically similar to annual averages (Peeters *et al*., 2002; Haddout *et al*., 2018). Shell taphonomy is also poorly understood, so isotopic compositions may be influenced by post-depositional events such as dissolution, coating, and vertical movement within sediment (Williams & Mellor, 1991).

Lake $\delta^{18}O_w$ appears to be the dominant driver of $\delta^{18}O_c$, rather than lake temperature (Figure 12). Unlike the tufas, inferred lake $\delta^{18}O_w$ does not correlate strongly with T_{47}, suggesting that the pre-evaporated lake water was not as constant as for the mound springs and had more variable $\delta^{18}O_w$. Variable $\delta^{18}O_w$ can probably be attributed to changes in lake volume, amount of precipitation, and precipitation $\delta^{18}O$ (Beuning *et al*., 2002; Evans *et al*., 2018). Central Australia ephemeral lakes are characterised by large degrees of evaporation, which impart a large signal on lake water $\delta^{18}O$. Variable $\delta^{18}O_w$ can also be attributed to lake water replenishment in seasonal pulses, rather than constantly, as with mound springs.

Despite limited samples, higher $\delta^{18}O_w$ corresponds with higher T_{47}, in agreement with an expected relationship between temperature and evaporation (Schaffner & Swart, 1991; Koch, 1998; Srivastava *et al.*, 2015; Miller & Fogel, 2016). However, this relationship is not particularly strong, and two samples exhibit higher temperatures than expected (Figure 12). A simple interpretation of these data would suggest that the lake was warmer, yet lake water was less evaporated or more diluted by fresh rainwater. Thus, a tentative interpretation could be that these two samples correspond with warmer and wetter climates, as compared to warmer and dryer climates for the other samples. This interpretation is supported by periods of lake filling during 33-31 ka and 50-40 ka coinciding with these warmer samples (Magee *et al*., 2004; Cohen *et al*., 2012, 2015), denoting periods of wetter climate.

5.4 Late Quaternary palaeoclimate implications

Whilst limited in number, palaeotemperature estimates produced in this study provide valuable insight into the past climate of central Australia, for which local proxy data is greatly required. This study provides the first clumped isotope estimates of central Australian temperatures during the last glacial period (Figure 15), paving the way for future work to extend this record in greater detail and length.

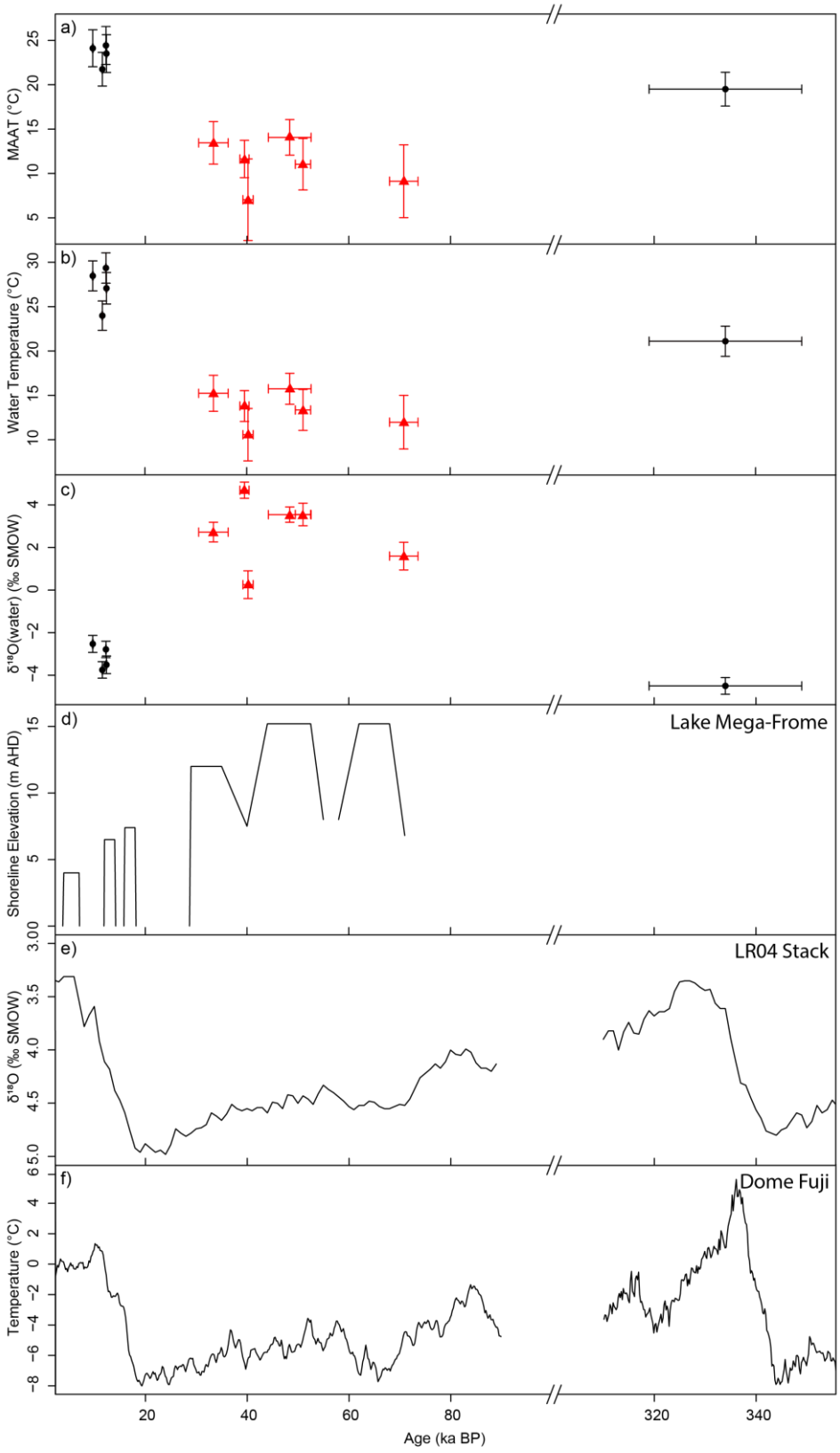

Figure 15: Comparison of central Australian palaeoclimate records from this study with previous palaeoclimate data. Clumped isotope proxy data for a) MAAT; b) water temperature; and c) water $\delta^{18}O$ from this study. Mound spring tufa samples are indicted by black circles, while lake mollusc samples are indicated by red triangles. d) Reconstructed shoreline elevation for Lake Mega-Frome

(Cohen *et al*., 2012). e) "LR04" stacked (averaged) benthic $\delta^{18}O$ record (Lisiecki & Raymo, 2005). f) Reconstructed temperature from ice core water isotopes at Dome Fuji, Antarctica (Uemura *et al*., 2012).

Lake shells suggest a MAAT of ~12 ± 3°C at ~71 ka, representing a palaeoclimate ~17°C cooler than modern climatic conditions. Central Australian MAAT appears to be largely stable throughout the next ~35 ka, with two periods of warmer climate during ~48 ka and ~33 ka, coinciding with periods of increased lake depth (Figure 15d). These two warmer periods correspond to periods of hydrological change in Lake Callabonna, as implied by a poor correlation between lake water temperature and $\delta^{18}O$.

By 12.4-9.7 ka, reconstructed central Australian climate was markedly warmer than during 70-33 ka (Figure 15a), with MAAT values ~5°C cooler than modern climate conditions. MAAT values during this period are supported by palaeotemperature values predicted by PaleoView (Fordham *et al*., 2017) (Figure 14) and previous air temperature estimates by Miller *et al*. (1997). Interpretation of palaeoclimate from tufa isotopic compositions is complicated by uncertainty regarding the isotopic composition of GAB groundwaters, although pre-evaporated spring water $\delta^{18}O$ appears to be consistent during 12.4-9.7 ka.

The data demonstrate a major glacial-interglacial temperature shift of ~10-12°C (Figure 15a). This shift is comparable with many studies worldwide (Shakun & Carlsen, 2010), although is greater than the global and Southern Hemisphere averages of ~4.0-3.5°C during this period (Shakun *et al*., 2012; Tierney *et al*., 2020). Mollusc samples indicate MAAT of 10-15°C, representing more significant cooling than models predict, although the inferred glacial-interglacial temperature range is comparable to that of Antarctica

(Petit *et al*., 1999; Uemura *et al*., 2012). Although subtle, there are two cooler shell MAAT values that may correspond to Antarctic temperature minima (Figure 15f) and lake emptying (Figure 15d) at ~70 and ~40 ka, suggesting that these samples may reflect more short-lived cooling episodes.

The cooler climates suggested by mollusc samples may suggest processes inherent in the large lake systems, which might act to lower spring/summer maximum temperatures or have lost heat via evaporation. Lakes generate specific climate features and are important for local weather formation due to the large difference in temperature between lake water and the surrounding land (Haddout *et al*., 2018). Cloud cover could have been greater due to increased moisture, resulting in lower temperatures (Kiem *et al*., 2016; Formayer & Fritz, 2017). The role of temperature with regards to evapotranspiration is debated in Australian, with water availability strongly coupled to temperature dynamics (Murphy & Timbal, 2008; Teuling *et al*., 2013). However, as noted by Kiem *et al.* (2016), our understanding of large-scale relationships between temperature and water sources is in its infancy. This may suggest the possibility of a bias in the perception of Australian glacial periods towards our modern view of the continental arid interior, with cooler climates able to promote lower evaporation, and thus the retention of water in the region.

The combination of warming and drying in central Australia could lead to exacerbated temperature rise, and possibly therefore the larger than expected magnitude of warming suggested by the data. Crucially, as the multitude of studies into Australian ecological and climatic change are largely based on near-coastal reconstructions of palaeoclimate,

dramatic changes in the arid interior due to the amplification of warming by drying may have major implications for the effects of climate on ecosystems and habitability.

5.5 Future research

Whilst this study provides the first tentative steps for clumped isotope research on the Quaternary carbonates of central Australia, several avenues of research must be pursued to ensure the reliability of palaeoclimate inferences. Foremost is the need for additional Δ_{47} analyses, especially for modern samples and during periods of overlap between tufa and mollusc samples, thus enabling comparison between the two proxies and increasing confidence in palaeoclimate shifts through time. Future mollusc studies should consider analysing a greater number of shells per sample, to provide a more time-averaged insight into palaeoclimate. As the term 'climate' is conventionally defined as the 30-year average of weather conditions (Mach *et al*., 2014) and sampled organisms are assumed to live for one year, sampling of ≥ 30 individuals would be ideal for ensuring relevant palaeoclimate data. Additional carbonate materials, such as pedogenic carbonate and ancient soil biota, may also be explored in future studies.

Additional research into spring morphology and GAB groundwater flow may be valuable for interpreting tufa Δ_{47}. Studies into gastropod ecology and shell taphonomy in the central Australian salt lakes may also be valuable for better understanding their Δ_{47}-inferred climatic conditions. If the depth at which *Coxiella* lived within central Australian lakes can be inferred, a 1D water temperature model could be applied to assess the potential difference between lake and air temperature (Haddout *et al*., 2018).

Whilst Δ_{47} data from both laboratories have been represented on the same absolute scale and are theoretically directly comparable, the possibility of instrument-specific effects may generate offsets in calculated temperatures for the same sample of up to 10°C (Dennis *et al*., 2011). Although, the same laboratory has been used for each sample type (tufa or lake shell), interlaboratory differences must be assessed through the analysis of identical samples at the UoA and other international laboratories, including the UoM.

Development of a method that allows the simultaneous high precision measurement of Δ_{47} and Δ_{48} isotopologues would enable the assessment of kinetic effects during carbonate precipitation, possibly alleviating concerns of tufa precipitation in disequilibrium with spring water. Research into the relationship between carbonate mineralisation rate and the incorporation of other elements or isotopes may be worthy of exploration. XRF analysis may be aided by elemental quantification software that is suitable for multiple mineral phases within tufa layers, although this is unlikely to fully resolve the observed similarities in good and poor ages.

6. CONCLUSIONS

This study provides the first attempt to infer past temperatures and hydroclimate of central Australia during the last glacial period using clumped isotope analysis of tufa and shell carbonates. Firstly, the study demonstrated the value of using XRF mapping to assess the nature and quality of tufa carbonate for U-series dating and clumped isotope analysis, whereby the principal concern is the avoidance of high magnesium (possibly dolomite) carbonate. Secondly, clumped isotope analysis of tufa and lake mollusc samples demonstrates significantly cooler air temperatures during the last glacial period. Despite the infancy of the work, this is arguably the most convincing and

comprehensive estimate of last glacial temperatures for central Australia. MAAT values are largely consistent with previous palaeotemperature reconstructions for the region, with a glacial-interglacial shift of ~10°C similar to several other locations worldwide, including Antarctica, although warming may have been exacerbated by the interplay between global climate and regional water. These findings suggest that clumped isotope analysis may serve as a novel quantitative proxy of past mean annual air temperatures in central Australia. While additional analyses are needed to refine and reinforce the findings of this thesis, the data highlight significant potential of the method, and raise important questions about the magnitude of glacial-interglacial climate shifts in arid central Australia.

ACKNOWLEDGMENTS

There are many people that I would like to thank for their assistance throughout this project. Firstly, I would like to thank my supervisors, Jonathan Tyler and Stacey Priestley, for their guidance during this Honours thesis, as well as their support with statistical analysis and palaeoenvironmental research. I would also like to thank Rob Klaebe, Tim Pollard and Russell Drysdale for assistance with isotopic analysis, Tony Hall for assistance with XRD, and Ben Wade, Sarah Gilbert, and Adelaide Microscopy for access to their micro-XRF scanner. I would like to thank Tim Cohen, Laura Crossey, Karl Karlstrom, and Andy Love for generously providing sample materials and additional data for this project, along with Damien Fordham for assistance with running PaleoView software. I would like to express my gratitude to Derrick Hasterok and Katie Howard for their organisation of the Honours program. I also wish to thank the good people of Tri-Star Group and the Playford Trust for financial support throughout the year.

I would like to acknowledge and thank the traditional owners and custodians (past and present) of the land from which samples were sourced, particularly the Arabana, Dhirari, and Pirlatapa peoples.

REFERENCES

AFFEK, H. P. & ZAARUR, S. (2014). Kinetic isotope effect in CO_2 degassing: Insight from clumped and oxygen isotopes in laboratory precipitation experiments. *Geochimica et Cosmochimica Acta*, 143, 319–330. https://doi.org/10.1016/j.gca.2014.08.005

ANDERSON, N. T., KELSON, J. R., KELE, S., DAËRON, M., BONIFACIE, M., HORITA, J., MACKEY, T. J., JOHN, C. M., KLUGE, T., PETSCHNIG, P., JOST, A. B., HUNTINGTON, K. W., BERNASCONI, S. M. & BERGAMANN, K. D. (2021). A unified clumped isotope thermometer calibration (0.5-1000°C) using carbonate-based standardization. *Geophysical Research Letters*, 48(7). https://doi.org/10.1029/2020GL092069

ANDREWS, J. E. (2006). Palaeoclimatic records from stable isotopes in riverine tufas: Synthesis and review. *Earth-Science Reviews*, 75(1), 85–104. https://doi.org/10.1016/j.earscirev.2005.08.002

ASMEROM, Y., POLYAK, V. J. & BURNS, S. J. (2010). Variable winter moisture in the southwestern United States linked to rapid glacial climate shifts. *Nature Geoscience*, 3(2), 114–117. https://doi.org/10.1038/NGEO754

ASMEROM, Y., POLYAK, V. J., SCHWIETERS, J. & BOUMAN, C. (2006). Routine high-precision U-Th isotope analyses for paleoclimate chronology. *Geochimica et Cosmochimica Acta*, 70, A24. https://doi.org/10.1016/j.gca.2006.06.061

AYLIFFE, L. K., MARIANELLI, P. C., MORIARTY, K. C., WELLS, R. T., MCCULLOCH, M. T., MORTIMER, G. E. & HELLSTROM, J. C. (1998). 500 ka precipitation record from southeastern Australia: Evidence for interglacial relative aridity. *Geology*, 26(2), 147–150. https://doi.org/10.1130/0091-7613(1998)026<0147:KPRFSA>2.3.CO;2

BAJNAI, D., GUO, W. F., SPOTL, C., COPLEN, T. B., METHNER, K., LOFFLER, N., KRSNIK, E., GISCHLER, E., HANSEN, N., HENKEL, D., PRICE, G. D., RADDATZ, J., SCHOLZ, D. & FIEBIG, J. (2020). Dual clumped isotope thermometry resolves kinetic biases in carbonate formation temperatures. *Nature Communications*, 11(1). https://doi.org/10.1038/s41467-020-17501-0

BERNASCONI, S. M., DAËRON, M., BERGMANN, K. D., BONIFACIE, M., MECKLER, A. N., AFFEK, H. P., ANDERSON, N., BAJNAI, D., BARKAN, E., BEVERLY, E., BLAMART, D., BURGENER, L., CALMELS, D., CHADUTEAU, C., CLOG, M., DAVIDHEISER-KROLL, B., DAVIES, A., DUX, F., EILER, J., ELLIOTT, B., FETROW, A. C., FIEBIG, J., GOLDBERG, S., HERMOSO, M., HUNTINGTON, K. W., HYLAND, E., INGALLS, M., JAGGI, M., JOHN, C. M., JOST, A. B., KATZ, S., KELSON, J., KLUGE, T., KOCKEN, I. J., LASKAR, A., LEUTERT, T. J., LIANG, D., LUCARELLI, J., MACKEY, T. J., MANGENOT, X., MEINICKE, N., MODESTOU, S. E., MÜLLER, I. A., MURRAY, S., NEARY, A., PACKARD, N., PASSEY, B. H., PELLETIER, E., PETERSEN, S., PIASECKI, A., SCHAUER, A., SNELL, K. E., SWART, P. K., TRIPATI, A., UPADHYAY, D., VENNEMANN, T., WINKELSTERN, I., YARIAN, D., YOSHIDA, N., ZHANG, N. & ZIEGLER, M. (2021). InterCarb: A community effort to improve interlaboratory standardization of the carbonate clumped isotope thermometer using carbonate standards. *Geochemistry, Geophysics, Geosystems*, 22(5), e2020GC009588. https://doi.org/ 10.1029/2020GC009588

BERNASCONI, S. M., HU, B., WACKER, U., FIEBIG, J., BREITENBACH, S. F. M. & RUTZ, T. (2013). Background effects on Faraday collectors in gas-source mass spectrometry and implications for clumped isotope measurements. *Rapid Communications in Mass Spectrometry*, 27(5), 603–612. https://doi.org/10.1002/rcm.6490

BERNASCONI, S. M., MÜLLER, I. A., BERGMANN, K. D., BREITENBACH, S. F. M., FERNANDEZ, A., HODELL, D. A., JAGGI, M., MECKLER, A. N., MILLAN, I. & ZIEGLER, M. (2018). Reducing uncertainties in carbonate clumped isotope analysis through consistent carbonate-based standardization. *Geochemistry, Geophysics, Geosystems* 19(9), 2895–2914. https://doi.org/10.1029/2017GC007385

BEUNING, K. R. M., KELTS, K., RUSSELL, J. & WOLFE, B. B. (2002). Reassessment of Lake Victoria–Upper Nile River paleohydrology from oxygen isotope records of lake-sediment cellulose. *Geology*, 30(6), 559–562. https://doi.org/10.1130/00917613(2002)030<0559:ROLVUN>2.0.CO;2

BRAND, W. A., ASSONOV, S. S. & COPLEN, T. B. (2010). Correction for the ^{17}O interference in $\delta(^{13}C)$ measurements when analyzing CO_2 with stable isotope mass spectrometry (IUPAC Technical Report). *Pure and Applied Chemistry*, 82(8), 1719–1733. https://doi.org/10.1351/PAC-REP-09-01-05

BRAY, P. S., JONES, C. M., FALLON, S. J., BROCKS, J. J. & GEORGE, S. C. (2012). Radiocarbon analysis of halophilic microbial lipids from an Australian salt lake. *Quaternary Research*, 77, 104–109. https://doi.org/10.1016/j.yqres.2011.10.003

CHAFETZ, H. S. & FOLK, R. L. (1984). Travertines: Depositional morphology and the bacterially constructed constituents. *Journal of Sedimentary Petrology*, 54(1), 289–316.

CHEN, S., RYB, U., PIASECKI, A. M., LLOYD, M. K., BAKER, M. B. & EILER, J. M. (2019). Mechanism of solid-state clumped isotope reordering in carbonate minerals from aragonite heating experiments. *Geochimica et Cosmochimica Acta*, 258, 156–173. https://doi.org/10.1016/j.gca.2019.05.018

COHEN, T. J., JANSEN, J. D., GLIGANIC, L. A., LARSEN, J. R., NANSON, G. C., MAY, J.-H., JONES, B. G. & PRICE, D. M. (2015). Hydrological transformation coincided with megafaunal extinction in central Australia. *Geology*, 43(3), 195–198. https://doi.org/10.1130/G36346.1

COHEN, T. J., MEYER, M. C. & MAY, J.-H. (2017). Identifying extreme pluvials in the last millennia using optical dating of single grains of quartz from shorelines on Australia's largest lake. *The Holocene*, 28(1), 150–165. https://doi.org/10.1177/0959683617715700

COHEN, T. J., NANSON, G. C., JANSEN, J. D., JONES, B. G., JACOBS, Z., LARSEN, J. R., MAY, J.-H., TREBLE, P., PRICE, D. M. & SMITH, A. M. (2012). Late Quaternary mega-lakes fed by the northern and southern river systems of central Australia: Varying moisture sources and increased continental aridity. *Palaeogeography, Palaeoclimatology, Palaeoecology*, 356, 89–108. https://doi.org/10.1016/j.palaeo.2011.06.023

COHEN, T. J., ARNOLD, L. J., GÁZQUEZ, F., MAY, J.-H., MARX, S., JANKOWSKI, N., CADD, H., PARKER, A., JANSEN, J., FU, X., MEYER, M., WALDMANN, N., NANSON, G. C. & JONES, B. (in prep). New evidence of long-term climate change in Australia's arid interior. *Quaternary Science Reviews*.

COLHOUN, E. A. & FITZSIMMONS, S. J. (1990). Late Cainozoic glaciation in western Tasmania, Australia. *Quaternary Science Reviews*, 9(2–3), 199–216. https://doi.org/10.1016/0277-3791(90)90018-6

CROSSEY, L. J., FISCHER, T. P., PATCHETT, P. J., KARLSTROM, K. E., HILTON, D. R., NEWELL, D. L., HUNTOON, P., REYNOLDS, A. C. & DE LEEUW, G. A. M. (2006). Dissected hydrologic system at the Grand Canyon: Interaction between deeply derived fluids and plateau aquifer waters in modern springs and travertine. *Geology*, 34(1), 25–28. https://doi.org/10.1130/G22057.1

DAËRON, M. (2021). Full propagation of analytical uncertainties in Δ_{47} measurements. *Geochemistry, Geophysics, Geosystems*, 22(5), e2020GC009592. https://doi.org/10.1029/2020GC009592

DAËRON, M., BLAMART, D., PERAL, M. & AFFEK, H. P. (2016). Absolute isotopic abundance ratios and the accuracy of Δ_{47} measurements. *Chemical Geology*, 442, 83–96. https://doi.org/10.1016/j.chemgeo.2016.08.014

DAËRON, M., DRYSDALE, R. N., PERAL, M., HUYGHE, D., BLAMART, D., COPLEN, T. B., LARTAUD, F. & ZANCHETTA, G. (2019). Most Earth-surface calcites precipitate out of isotopic equilibrium. *Nature Communications*, 10(429). https://doi.org/10.1038/s41467-019-08336-5

DE DECKKER, P. & LAST, W. M. (1988). Modern dolomite deposition in continental, saline lakes, western Victoria, Australia. *Geology*, 16(1), 29–32. https://doi.org/10.1130/0091-7613(1988)016<0029:MDDICS>2.3.CO2

DE DECKKER, P., MAGEE, J. W. & SHELLEY, J. M. G. (2011). Late Quaternary palaeohydrological changes in the large playa Lake Frome in central Australia, recorded from the Mg/Ca and Sr/Ca in ostracod valves and biotic remains. *Journal of Arid Environments*, 75(1), 38–50. https://doi.org/10.1016/j.jaridenv.2010.08.004

DEFLIESE, W. F., HREN, M. T. & LOHMANN, K. C. (2015). Compositional and temperature effects of phosphoric acid fractionation on Δ_{47} analysis and implications for discrepant calibrations. *Chemical Geology*, 396, 51–60. https://doi.org/10.1016/j.chemgeo.2014.12.018

DENNIS, K. J., AFFEK, H. P., PASSEY, B. H., SCHRAG, D. P. & EILER, J. M. (2011). Defining an absolute reference frame for 'clumped' isotope studies of CO_2. *Geochimica et Cosmochimica Acta*, 75, 7117–7131. https://doi.org/10.1016/j.gca.2011.09.025

DENNISTON, R. F., WYRWOLL, K. H., ASMEROM, Y., POLYAK, V. J., HUMPHREYS, W. F., CUGLEY, J., WOODS, D., LAPOINTE, Z., PEOTA, J. & GREAVES, E. (2013). North Atlantic forcing of millennial-scale Indo-Australian monsoon dynamics during the Last Glacial period. *Quaternary Science Reviews*, 72, 159–168. https://doi.org/10.1016/j.quascirev.2013.04.012

EILER, J. M. (2007). "Clumped-isotope" geochemistry – The study of naturally-occurring, multiply-substituted isotopologues. *Earth and Planetary Science Letters*, 262(3-4), 309–327. https://doi.org/10.1016/j.epsl.2007.08.020

ENGLISH, P., SPOONER, N. A., CHAPPELL, J., QUESTIAUX, D. G. & HILL, N. G. (2001). Lake Lewis basin, central Australia: environmental evolution and OSL chronology. *Quaternary International*, 83–85, 81–101. https://doi.org/10.1016/S1040-6182(01)00032-5

FACCENNA, C., SOLIGO, M., BILLI, A., DE FILIPPIS, L. & FUNICIELLO, R. (2008). Late Pleistocene depositional cycles of the Lapis Tiburtinus travertine (Tivoli, Central Italy): Possible

influence of climate and fault activity. *Global and Planetary Change*, 63, 299–308. https://doi.org/10.1016/j.gloplacha.2008.06.006

FALSTER, G., DELEAN, S., & TYLER, J. (2018). Hydrogen peroxide treatment of natural lake sediment prior to carbon and oxygen stable isotope analysis of calcium carbonate. *Geochemistry, Geophysics, Geosystems*, 19, 3583–3595. https://doi.org/10.1029/2018GC007575

FALSTER, G., TYLER, J., DUX, F., KLUGE, T., DRYSDALE, R., TIBBY, J. & REED, L. (2019). Clumped isotopes in freshwater snail shells: A new quantitative temperature proxy for Australia, and its application to fossil *Glyptophysa* shells from Blanche Cave. PhD thesis, University of Adelaide.

FIEBIG, J., BAJNAI, D., LOFFLER, N., METHNER, K., KRSNIK, E., MULCH, A. & HOFMANN, S. (2019). Combined high-precision Δ_{48} and Δ_{47} analysis of carbonates. *Chemical Geology*, 522, 186–191. https://doi.org/10.1016/j.chemgeo.2019.05.019

FITZSIMMONS, K. E., COHEN, T. J., HESSE, P. P., JANSEN, J., NANSON, G. C., MAY, J.-H., BARROWS, T. T., HABERLAH, D., HILGERS, A., KELLY, T., LARSEN, J., LOMAX, J. & TREBLE, P. (2013). Late Quaternary palaeoenvironmental change in the Australian drylands. *Quaternary Science Reviews*, 74, 78–96. https://doi.org/10.1016/j.quascirev.2012.09.007

FORD, T. D. & PEDLEY, H. M. (1996). A review of tufa and travertine deposits of the world. *Earth-Science Reviews*, 41, 117–175. https://doi.org/10.1016/S0012-8252(96)00030-X

FORMAYER, H. & FRITZ, A. (2017). Temperature dependency of hourly precipitation intensities – surface versus cloud layer temperature. *International journal of climatology*, 37(1), 1–10. https://doi.org/10.1002/joc.4678

GALLOWAY, R. F. (1965). Late Quaternary Climates in Australia. *Journal of Geology*, 73(4), 603–618.

GHOSH, P., ADKINS, J., AFFEK, H., BALTA, B., GUO, W., SCHAUBLE, E. A., SCHRAG, D. & EILER, J. M. (2006). ^{13}C–^{18}O bonds in carbonate minerals: A new kind of paleothermometer. *Geochimica et Cosmochimica Acta*, 70, 1439–1456. https://doi.org/10.1016/j.gca.2005.11.014

GILGANIC, L. A., COHEN, T. J., MAY, J.-H., JANSEN, J. D., NANSON, G. C., DOSSETO, A., LARSEN, J. R. & AUBERT, M. (2014). Late-Holocene climatic variability indicated by three natural archives in arid southern Australia. *The Holocene*, 24(1), 104–117. https://doi.org/10.1177/0959683613515732

GIMENO, L., DRUMOND, A., NIETO, R., TRIGO, R. M. & STOHL, A. (2010). On the origin of continental precipitation. *Geophysical Research Letters*, 37, L13804. https://doi.org/10.1029/2010GL043712

GUO, Y. R., DENG, W. F. & WEI, G. J. (2019). Kinetic effects during the experimental transition of aragonite to calcite in aqueous solution: Insights from clumped and oxygen isotope signatures. *Geochimica et Cosmochimica Acta*, 248, 210–230. https://doi.org/10.1016/j.gca.2019.01.012

HADDOUT, S., PRIYA, K. L., BOKO, M. & AZIDANE, H. (2018). Comparison of one-dimensional (1-D) column lake models prediction for surface water temperature in eight selected Moroccan lakes, *ISH Journal of Hydraulic Engineering*, 24(3), 317–329, https://doi.org/10.1080/09715010.2017.1376294

HANCOCK, P. L., CHALMERS, R. M. L., ALTUNEL, E. & ÇAKIR, Z. (1999). Travitonics: Using travertines in active fault studies. *Journal of Structural Geology*, 21(8-9), 903–916. https://doi.org/10.1016/S0191-8141(99)00061-9

HENKES, G. A, PASSEY, B. H., WANAMAKER JR., A. D., GROSSMAN, E. L., AMBROSE JR., W. G. & CARROLL, M. L. (2013). Carbonate clumped isotope compositions of modern marine mollusk and brachiopod shells. *Geochimica et Cosmochimica Acta*, 106, 307–325. https://doi.org/10.1016/j.gca.2012.12.020

HESSE, P. P., MAGEE, J. W. & VAN DER KAARS, S., 2004. Late Quaternary climates of the Australian arid zone: A review. *Quaternary International*, 118, 87–102. https://doi.org/10.1016/S1040-6182(03)00132-0

HREN, M. T. & SHELDON, N. D. (2012). Temporal variations in lake water temperature: Paleoenvironmental implications of lake carbonate δ18O and temperature records. *Earth and Planetary Science Letters*, 337, 77–84. https://doi.org/10.1016/j.epsl.2012.05.019

HUNTINGTON, K. W., EILER, J. M., AFFEK, H. P., GUO, W., BONIFACIE, M., YEUNG, L. Y., THIAGARJAN, N., PASSEY, B., TRIPATI, A., DAËRON, M. & CAME, R. (2009). Methods and limitations of 'clumped' CO_2 isotope (Δ_{47}) analysis by gas-source isotope ratio mass spectrometry. *Journal of Mass Spectrometry*, 44(9), 1318–1329. https://doi.org/10.1002/jms.1614

KATO, H., AMEKAWA, S., KANO, A., MORI, T., KUWAHARA, Y. & QUADE, J. (2019). Seasonal temperature changes obtained from carbonate clumped isotopes of annually laminated tufas from Japan: Discrepancy between natural and synthetic calcites. *Geochimica et Cosmochimica Acta*, 244, 548–564. https://doi.org/10.1016/j.gca.2018.10.016

KELE, S., BREITENBACH, S. F. M., CAPEZZUOLI, E., MECKLER, A. N., ZIEGLER, M., MILLAN, I. M., KLUGE, T., DEÁK, J., HANSELMANN, K., JOHN, C. M., YAN, H., LIU, Z. & BERNASCONI, S. M. (2015). Temperature dependence of oxygen- and clumped isotope fractionation in carbonates: A study of travertines and tufas in the 6–95 °C temperature range. *Geochimica et Cosmochimica Acta*, 168, 172–192. https://doi.org/10.1016/j.gca.2015.06.032

KELE, S., ÖZKUL, M., FÓRIZS, I., GÖKGÖZ, A., BAYKARA, M. O., ALÇIÇEK, M. C. & NÉMETH, T. (2011). Stable isotope geochemical study of Pamukkale travertines: New evidences of low-temperature non-equilibrium calcite-water fractionation. *Sedimentary Geology*, 238(1-2), 191–212. https://doi.org/10.1016/j.sedgeo.2011.04.015

KELSON, J. R., HUNTINGTON, K. W., SCHAUER, A. J., SAENGER, C. & LECHLER, A. R. (2017). Toward a universal carbonate clumped isotope calibration: Diverse synthesis and preparatory methods suggest a single temperature relationship. *Geochimica et Cosmochimica Acta*, 197, 104–131. https://doi.org/10.1016/j.gca.2016.10.010

KEPPEL, M. N., CLARKE, J. D. A., HALIHAN, T., LOVE, A. J. & WERNER, A. D. (2011). Mound springs in the arid Lake Eyre South region of South Australia: A new depositional tufa model and its controls. *Sedimentary Geology*, 240(3-4), 55–70. https://doi.org/10.1016/j.sedgeo.2011.08.001

KEPPEL, M. N., POST, V. E. A., LOVE, A. J., CLARKE, J. D. A. & WERNER, A. D. (2012). Influences on the carbonate hydrochemistry of mound spring environments, Lake Eyre South region, South Australia. *Chemical Geology*, 296, 50–65. https://doi.org/10.1016/j.chemgeo.2011.12.017

KERSHAW, A. P. (1994). Pleistocene vegetation of the humid tropics of northeastern Queensland, Australia. *Paleogeography, Palaeoclimatology, Palaeoecology*, 109, 39–412.

KIEM, A. S., JOHNSON, F., WESTRA, S., VAN DIJK, A., EVANS, JASON P., O'DONNELL, A., ROUILLARD, A., BARR, C., TYLER, J., THYER, M., JAKOB, D., WOLDEMESKEL, F., SIVAKUMAR, B., MEHROTRA, R., WESTRA, S., WHITE, C. J. & KIEM, A. (2016). Natural hazards in Australia: Droughts. *Climatic Change*, 139(1), 37–54. https://doi.org/10.1007/s10584-016-1798-7

KIM, S. T. & O'NEIL. (1997). Equilibrium and nonequilibrium oxygen isotope effects in synthetic carbonates. *Geochimica et Cosmochimica Acta*, 61(16), 3461–3475. https://doi.org/10.1016/S0016-7037(97)00169-5

KIM, S. T., O'NEIL, J. R., HILLAIRE-MARCEL, C. & MUCCI, A. (2007). Oxygen isotope fractionation between synthetic aragonite and water: Influence of temperature and Mg^{2+} concentration. *Geochimica et Cosmochimica Acta*, 71(19), 4704-4715. https://doi.org/10.1016/j.gca.2007.04.019

KOCH, P. L. (1998). Isotopic reconstruction of past continental environments. *Annual Review of Earth and Planetary Sciences*, 26, 573–613. https://doi.org/ 10.1146/annurev.earth.26.1.573

KOCKEN, I. J., MÜLLER, I. A. & ZIEGLER, M. (2019). Optimizing the Use of Carbonate Standards to Minimize Uncertainties in Clumped Isotope Data. *Geochemistry, Geophysics, Geosystems*, 20(11), 5565–5577. https://doi.org/10.1029/2019GC008545

LOVE, A. J., WOHLING, D., FULTON, S., ROUSSEAU-GUEUTIN, P. & DE RITTER, S. (2013). Allocating water and maintaining springs in the Great Artesian Basin, Volume II: Groundwater Recharge, Hydrodynamics and Hydrochemistry of the Western Great Artesian Basin. *National Water Commission, Canberra.*

MACH, K. J., PLANTON, S. & STECHOW, C. V. (2014). IPCC 2014 Annex II: Glossary. In: PACHAURI, R. K. & MEYER, L.A. (Eds.), *Climate Change 2014: Synthesis Report. Contribution of Working Groups I, II and III to the Fifth Assessment Report of the Intergovernmental Panel on Climate Change* (pp. 117–130). IPCC, Geneva, Switzerland.

MAGEE, J. W., MILLER, G. H., SPOONER, N. A. & QUESTIAUX, D. (2004). A continuous 150 k.y. monsoon record from Lake Eyre, Australia: Insolation-forcing implications and unexpected Holocene failure. *Geology*, 32(10), 885–888. https://doi.org/10.1130/G20672.1

MAHARA, Y., HABERMEHL, M. A., HASEGAWA, T., NAKATA, K., RANSLEY, T. R., HATANO, T., MIZUOCHI, Y., KOBAYASHI, H., NINOMIYA, A., SENIOR, B. R., YASUDA, H. & OHTA, T. (2009). Groundwater dating by estimation of groundwater flow velocity and dissolved ^{4}He accumulation rate calibrated by ^{36}Cl in the Great Artesian Basin, Australia. *Earth Planetary Science Letters*, 287(1-2), 43–56. https://doi.org/10.1016/j.epsl.2009.07.034

MAY, J.-H., BARRETT, A., COHEN, T. J., JONES, B. G., PRICE, D. & GLICANIC, L. A. (2015). Late Quaternary evolution of a playa margin at Lake Frome, South Australia. *Journal of Arid Environments*, 122, 93–108. https://doi.org/10.1016/j.jaridenv.2015.06.012

MECKLER, A. N., ZIEGLER, M., MILLAN, M. I., BREITENBACH, F. M. & BERNASCONI, S. M. (2014). Long-term performance of the Kiel carbonate device with a new correction scheme for clumped isotope

measurements. *Rapid Communications in Mass Spectrometry*, 28(15), 1705–1715. https://doi.org/10.1002/rcm.6949

MILLER, G. H. & FOGEL, M. L. (2016). Calibrating d18O in *Dromaius novaehollandiae* (emu) eggshell calcite as a paleo-aridity proxy for the Quaternary of Australia. *Geochimica et Cosmochimica Acta*, 193, 1–13. https://doi.org/10.1016/j.gca.2016.08.004

MILLER, G. H., FOGEL, M. L., MAGEE, J. W. & GAGAN, M. K. (2016). Disentangling the impacts of climate and human colonization on the flora and fauna of the Australian arid zone over the past 100 ka using stable isotopes in avian eggshell. *Quaternary Science Reviews*, 151, 27–57. https://doi.org/10.1016/j.quascirev.2016.08.009

MILLER, G. H., MAGEE, J. W. & JULL, J. T. (1997). Low-latitude glacial cooling in the Southern Hemisphere from amino-acid racemization in emu eggshells. *Nature*, 385(6613), 241–244. https://doi.org/10.1038/385241a0

MÜLLER, I. A., VIOLAY, M. E. S., STORCK, J.-C., FERNANDEZ, A., VAN DIJK, J., MADONNA, C. & BERNASCONI, S. M. (2017). Clumped isotope fractionation during phosphoric acid digestion of carbonates at 70 °C. *Chemical Geology*, 449, 1–14. https://doi.org/10.1016/j.chemgeo.2016.11.030

MURPHY, B. F. & TIMBAL, B. (2008). A review of recent climate variability and climate change in southeastern Australia. *International Journal of Climatology*, 28(7), 859–879. https://doi.org/10.1002/joc.1627

NANSON, G. C., PRICE, D. M., JONES, B. G., MAROULIS, J. C., COLEMAN, M., BOWMAN, H., COHEN, T. J., PIETSCH, T. J. & LARSEN, J. R. (2008). Alluvial evidence for major climate and flow regime changes during the middle and late Quaternary in eastern central Australia. *Geomorphology*, 101(1-2), 109–129. https://doi.org/10.1016/j.geomorph.2008.05.032

OKSANEN, J., BLANCHET, F. G., KINDT, R., LEGENDRE, P., MINCHIN, P., O'HARA, R. B., SIMPSON, G., SOLYMOS, P., STEVENS, M. H. H. & WAGNER, H. (2013). Vegan: Community ecology package. R package version. 2.0-10. CRAN.

PASSEY B. H. & HENKES G. A. (2012). Carbonate clumped isotope bond reordering and geospeedometry. *Earth and Planetary Science Letters*, 351, 223–236. https://doi.org/10.1016/j.epsl.2012.07.021.

PEARSON, S., SEARSON, M. & GAYLER, L. (2001). Preliminary results from tree increment and playa sediment cores from the Paroo, north-western New South Wales, Australia. *Quaternary International*, 83–85, 145–153. https://doi.org/10.1016/S1040-6182(01)00036-2

PEETERS, F., LIVINGSTONE, D. M., GOUDSMIT, G., KIPFER, R. & FORSTER, R. (2002). Modeling 50 years of historical temperature profiles in a large central European lake. *Limnology and Oceanography*, 47(1), 186–197. https://doi.org/10.4319/lo.2002.47.1.0186

PETERSEN, S. V., DEFLIESE., W. F., SAENGER, C., DAËRON, M., HUNTINGTON, K. W., JOHN, C. M., KELSON, J. R., BERNASCONI, S. M., COLMAN, A. S., KLUGE, T., OLACK, G. A., SCHAUER, A. J., BAJNAI, D., BONIFACIE, M., BREITENBACH, S. F. M., FIEBIG, J., FERNANDEZ, A. B., HENKES, G. A., HODELL, D., KATZ, A., KELE, S., LOHMANN, K. C., PASSEY, B. H., PERAL, M. Y., PETRIZZO, D. A., ROENHEIM, B. E., TRIPATI, A., VENTURELLI, R., YOUNG, E. D. & WINKELSTERN, I. Z. (2019). Effects of improved ^{17}O correction on interlaboratory agreement in clumped isotope calibrations, estimates of mineral-specific offsets, and temperature dependence of acid digestion fractionation. *Geochemistry, Geophysics, Geosystems*, 20(7), 3495–3519. https://doi.org/10.1029/2018GC008127

PETERSEN, S. V., WINKELSTERN, I. Z., LOHMANN, K. C. & MEYER, K. W. (2016). The effects of Porapak™ trap temperature on $\delta^{18}O$, $\delta^{13}C$, and Δ_{47} values in preparing samples for clumped isotope analysis. *Rapid Communications in Mass Spectrometry*, 30(1), 199–208. https://doi.org/10.1002/rcm.7438

PETIT, J. R., JOUZEL, J., RAYNAUD, D., BARKOV, N. I., BARNOLA, J.-M., BASILE, I., BENDER, M., CHAPPELLAZ, J., DAVIS, M., DELAYGUE, G., DELMOTTE, M., KOTLYAKOV, V. M., LEGRAND, M., LIPENKOV, V. Y., LORIUS, C., PÉPIN, L., RITZ, C., SALTZMAN, E. & STIEVENARD, M. (1999). Climate and atmospheric history of the past 420,000 years from the Vostok ice core, Antarctica. *Nature (London)*, 399(6735), 429–436. https://doi.org/10.1038/20859

PRIESTLEY, S. C., KARLSTROM, K. E., LOVE, A. J., CROSSEY, L. J., POLYAK, V. J., ASMEROM, Y., MEREDITH, K. T., CROW, R., KEPPEL, M. N. & HABERMEHL, M. A. (2018). Uranium series dating of Great Artesian Basin travertine deposits: Implications for palaeohydrogeology and palaeoclimate. *Palaeogeography, Palaeoclimatology, Palaeoecology*, 490, 163–177. https://doi.org/10.1016/j.palaeo.2017.10.024

RADKE, B. M., FERGUSON, J., CRESSWELL, R. G., RANSLEY, T. R. & HABERMEHL, M. A. (2000). *Hydrochemistry and Implied Hydrodynamics of the Cadna-Owie - Hooray Aquifer, Great Artesian Basin, Australia*. Bureau of Rural Sciences, Canberra.

REEVES, J. M., BARROWS, T. T., COHEN, T. J., KIEM, A. S., BOSTOCK, H. C., FITZSIMMONS, K. E., JANSEN, J. D., KEMP, J., KRAUES, C., PETHERICK, L. & PHIPPS, S. J. (2013). Climate variability over the last 35,000 years recorded in marine and terrestrial archives in the Australian region: An OZ-INTIMATE compilation. *Quaternary Science Reviews*, 74, 21–34. https://doi.org/10.1016/j.quascirev.2013.01.001

ROBERTS, L. R., HOLMES, J. A., LENG, M. J., SLOANE, H. J. & HOME, D. J. (2018). Effects of cleaning methods upon preservation of stable isotopes and trace elements in shells of *Cyprideis torosa* (Crustacea, Ostracoda): Implications for palaeoenvironmental reconstruction. *Quaternary Science Reviews*, 189, 197–209. https://doi.org/10.1016/j.quascirev.2018.03.030

ROUSSEAU-GUEUTIN, P., LOVE, A. J., VASSEUR, G., ROBINSON, N. I., SIMMONS, C. T. & DE MARSILY, G. (2013). Time to reach near-steady state in large aquifers. *Water Resources Research* 49(10), 6893–6908. https://doi.org/10.1002/wrcr.20534

SCHAFFNER, F. C. & SWART P. K. (1991). Influence of diet and environmental water on the carbon and oxygen isotopic signatures of seabird eggshell carbonate. *Bulletin of Marine Science*, 48(1), 23–38.

SHAKUN, J. D. & CARLSON, A. E. (2010). A global perspective on Last Glacial Maximum to Holocene climate change. *Quaternary Science Reviews*, 29(15), 1801–1816. https://doi.org/10.1016/j.quascirev.2010.03.016

SHAKUN, J. D., CLARK, P. U., HE, F., MARCOTT, S. A., MIX, A. C., LIU, Z., OTTO-BLIESNER, B., SCHMITTNER, A. & BARD, E. (2012). Global warming preceded by increasing carbon dioxide concentrations during the last deglaciation. *Nature*, 484(7392), 49–54. https://doi.org/10.1038/nature10915

SINGH, G. & GEISSLER, E. A. (1985). Late Cainozoic history of vegetation, fire, lake levels and climate, at Lake George, New South Wales, Australia. *Philosophical Transactions of the Royal Society B-Biological Sciences*, 311(1151), 379–447. https://doi.org/10.1098/rstb.1985.0156

SPENCER, C. & KIM, S.-T. (2015). Carbonate clumped isotope paleothermometry: a review of recent advances in CO_2 gas evolution, purification, measurement and standardization techniques. *Geosciences Journal*, 19(2), 357–374. https://doi.org/10.1007/s12303-015-0018-1

SRIVASTAVA, R., RAMESH, R., GANDHI, N., JANI, R. A. & SINGH, A. K. (2015). Monsoon onset signal in the stable oxygen and hydrogen isotope ratios of monsoon vapor. *Atmospheric Environment*, 108, 117–124. https://doi.org/10.1016/j.atmosenv.2015.02.062

STAUDIGEL, P. T. & SWART, P. K. (2016). Isotopic behavior during the aragonite-calcite transition: Implications for sample preparation and proxy interpretation. *Chemical Geology*, 442, 130–138. https://doi.org/10.1016/j.chemgeo.2016.09.013

TANG, J., DIETZEL, M., FERNANDEZ, A., TRIPATI, A. K. & ROSENHEIM, B. E. (2014). Evaluation of kinetic effects on clumped isotope fractionation (Δ_{47}) during inorganic calcite precipitation. *Geochimica et Cosmochimica Acta*, 134, 120–136. https://doi.org/10.1016/j.gca.2014.03.005

TEULING, A. J., VAN LOON, A. F., SENEVIRATNE, S. I., LEHNER, I., AUBINET, M., HEINESCH, B., BERNHOFER, C., GRÜNWALD, T., PRASSE, H. & SPANK, U. (2013). Evapotranspiration amplifies European summer drought. *Geophysical Research Letters*, 40(10), 2071–2075. https://doi.org/10.1002/grl.50495

TIMMS, B. V. (1976). A comparative study of the limnology of three maar lakes in western Victoria. I. Physiography and physiochemical features. *Marine and Freshwater Research*, 27(1), 35–60. https://doi.org/10.1071/MF9760035

TORGERSEN, T., HABERMEHL, M. A. & CLARKE, W. B. (1992). Crustal helium fluxes and heat flow in the Great Artesian Basin, Australia. *Chemical Geology*, 102(1-4), 139–152. https://doi.org/10.1016/0009-2541(92)90152-U

TORGERSEN, T., HABERMEHL, M. A., PHILLIPS, F. M., ELMORE, D., KUBIK, P., JONES, B. G., HEMMICK, T. & GOVE, H. E. (1991). Chlorine 36 dating of very old groundwater 3. Further studies in the Great Artesian Basin, Australia. *Water Resources Research*, 27(12), 3201–3213. https://doi.org/10.1029/91WR02078

TREBLE, P. C., BAKER, A., AYLIFFE, L. K., COHEN, T. J., HELLSTROM, J. C., GAGAN, M. K., FRISIA, S., DRYSDALE, R. N., GRIFFITHS, A. D. & BORSATO, A. (2017). Hydroclimate of the Last Glacial Maximum and deglaciation in southern Australia's arid margin interpreted from speleothem records (23-15 ka). *Climate of the Past*, 13(6), 667–687. https://doi.org/10.5194/cp-13-667-2017

TURNEY, C. S. M., KERSHAW, A. P., CLEMENS, S. C., BRANCH, N., MOSS, P. T. & FIFIELD, L. K. (2004). Millennial and orbital variations of El Nino/Southern Oscillation and high-latitude climate in the last glacial period. *Nature*, 428(6980), 306–310. https://doi.org/10.1038/nature02386

UEMURA, R., MASSON-DELMOTTE, V., JOUZEL, J., LANDAIS, A., MOTOYAMA, H. & STENNI, B. (2012). Ranges of moisture-source temperature estimated from Antarctic ice cores stable isotope records over glacial-interglacial cycles. *Climate of the Past*, 8(3), 1109–1125. https://doi.org/10.5194/cp-8-1109-2012

WANG, X., CUI, L., ZHAI, J. & DING, Z. (2016). Stable and clumped isotopes in shell carbonates of land snails *Cathaica* sp. and *Bradybaena* sp. in north China and implications for ecophysiological characteristics and paleoclimate studies. *Geochemistry, Geophysics, Geosystems*, 17(1), 219–231. https://doi.org/10.1002/2015GC006182

WANG, Y., PASSEY, B., ROY, R., DENG, T., JIANG, S., HANNOLD, C., WANG, X., LOCHNER, E. & TRIPATI, A. (2021). Clumped isotope thermometry of modern and fossil snail shells from the Himalayan-Tibetan Plateau: Implications for paleoclimate and paleoelevation reconstructions. Geological Society of America Bulletin, 133(7–8), 1370–1380. https://doi.org/10.1130/B35784.1

WILLIAMS, W. D & MELLOR, M. W. (1991). Ecology of *Coxiella* (Mollusca, Gastropoda, Prosobranchia), a snail endemic to Australian salt lakes. *Palaeogeography, Palaeoclimatology, Palaeoecology*, 84(1), 339–355. https://doi.org/10.1016/0031-0182(91)90053-T

WINKELSTERN, I. Z., KACZMAREK, S. E., LOHMANN, K. C. & HUMPHREY, J. D. (2016). Calibration of dolomite clumped isotope thermometry. *Chemical Geology*, 443, 32–38. https://doi.org/10.1016/j.chemgeo.2016.09.021

ZHANG, N. Z., LIN, M., YAMADA, K., KANO, A., LIU, Q., YOSHIDA, N. & MATSUMOTO, R. (2020). The effect of H_2O_2 treatment on stable isotope analysis ($\delta^{13}C$, $\delta^{18}O$ and Δ_{47}) of various carbonate minerals. *Chemical Geology*, 532, 119352. https://doi.org/10.1016/j.chemgeo.2019.119352

APPENDIX A: SITE DATA

Table A.1: Site location and type for mound spring carbonate samples

Sample ID	Sample area	Sample type	Easting	Northing	Elevation
			UTM GDA 53 J		(m) AHD[a]
BER 2	Beresford Spring	Micrite	661,606	6,761,595	25
BLAN A	Blanche cup	Micrite (?)	680,265	6,740,444	Not Recorded
DAL A	Dalhousie Springs	Micrite (?)	546,426	7,070,973	135
DAL 1A	Dalhousie Springs	Micrite	549,896	7,077,885	120
DAL 2A	Dalhousie Springs	Micrite	546,363	7,074,457	126
DAL 4C[b]	Dalhousie Springs	Infilling	550,819	7,076,289	127
DAL 5	Dalhousie Springs	Micrite	548,770	7,073,846	125
ELIZ A	Elizabeth Springs	Micrite (?)	672,021	6,751,868	29
ELIZ C	Elizabeth Springs	Infilling (?)	672,058	6,751,685	Not Recorded
ELIZ D	Elizabeth Springs	Micrite (?)	671,755	6,751,228	5
Eliz Sp	Elizabeth Springs	Infilling	671,640	6,751,681	46
Gosse	Gosse Spring	Micrite	726,701	6,738,648	-7
JER 3	Jersey Spring	Micrite (flow stone)	670,683	6,752,745	28
KEW 3	Kewson Hill	Infilling	672,470	6,749,873	27
SUL 1a[b]	Sulphuric Spring	Infilling	733,407	6,722,980	3
SUL 1b[b]	Sulphuric Spring	Infilling	733,407	6,722,980	3
SUL 1c[b]	Sulphuric Spring	Infilling	733,407	6,722,980	3
SUL 1d[b]	Sulphuric Spring	Infilling	733,407	6,722,980	3
SUL 1e[b]	Sulphuric Spring	Infilling	733,407	6,722,980	3
SUL 1f[b]	Sulphuric Spring	Infilling	733,407	6,722,980	3

WAR 1	Warburton Spring	Micrite	662,324	6,760,351	29
WAR 5	Warburton Hill	Micrite	- - - - - - - - - Not Recorded - - - - - - - - -		
WAR 7	Warburton Hill	Micrite	662,735	6,760,221	45

[a]AHD – Australian Height Datum, equivalent to metres above sea level

[b]samples used for clumped isotope analyses

Table A.2: Site location and type for mound spring carbonate samples

Sample ID	Sample area	Sample type	Shells Used (n)	Coordinates	Elevation (m) AHD[a]
LCP1 0.8	Lake Callabonna	*Coxiella sp.*	15	S 29° 56′22.45″ E 140° 6′46.86″	10.4
LCP2 0.85	Lake Callabonna	*Coxiella sp.*	10	S 29° 56′23.55″ E 140° 6′56.12″	7.0
LCP1 0.96	Lake Callabonna	Bivalve	1	S 29° 56′22.45″ E 140° 6′46.86″	10.4
CSP1 1.0	Lake Callabonna	*Coxiella sp.*	3	S 29° 48′25.67″ E 140° 4′19.69	15.4
CSP1 1.05	Lake Callabonna	*Coxiella sp.*	2	S 29° 48′25.67″ E 140° 4′19.69	15.4
WPLE P4B	Lake Eyre	*Coxiella sp.*	10	S 29° 2′16.15″ E 137° 37′45.31	Not Recorded

[a]AHD – Australian Height Datum, equivalent to metres above sea level

APPENDIX B: ADDITIONAL METHODS

B.1 XRF and XRD analyses

For the purposes of comparison of XRF data for tufas of varying U-series data quality, tufa samples were classified as "Good Age" or "Poor Age" samples by using thorium and uranium data from Priestley *et al*. (2018). Briefly, $^{230}Th/^{234}U$ and $^{230}Th/^{238}U$ activity ratios were used in conjunction with $^{230}Th/^{234}U$ or $^{230}Th/^{238}U$ and $^{234}U/^{238}U$ activity ratios to identify activity ratios that could not be attained through radioactive decay and must have resulted from open-system behaviour (Kaufman *et al*., 1971; Burnside, 2010; Priestley *et al*., 2018).

Minerology was determined by XRD analysis conducted qualitatively using a Bruker D8 ADVANCE Powder X-ray Diffractometer with a Cu-radiation source operating at 40KV and 40amps, scanning 2 theta from 5 to 65 degrees with sample rotation of 30 rotations per min. XRD was conducted in the Mawson Analytical Spectrometry

Services (MASS) Facilities, University of Adelaide. Sample powdered were sprinkled onto silicone wafers in a fine dusting over the centre of the wafer and loaded into an XRD sample holder with vibration to minimise orientation. Data was processed using Bruker DIFFRAC.EVA software and Crystallography Open Database reference patterns for identifying mineral phases.

B.2 Clumped isotope analyses

The extremely high precision and accuracy required for clumped isotope analysis was achieved through more extensive carbon dioxide purification than traditional stable isotope analyses (Ghosh *et al*., 2006; Eiler *et al*., 2007; Kocken *et al*., 2019). CO_2 was extracted from tufa and mollusc samples by digestion of carbonate with H_3PO_3 at a constant temperature. CO_2 purification was performed through the vacuum line by a combination of cryogenic and adsorptive means to remove possible contaminants, such as water, O_2, N_2, hydrocarbons, and halocarbons.

Clumped isotope analyses were performed at the University of Adelaide (UoA) (shell samples) and the University of Melbourne (UoM) (tufa samples) using identical methods. Samples were analysed using a Nu Instruments Perspective-IS stable isotope ratio mass spectrometer, interfaced with the Nu Carb carbonate sample preparation system. Sample aliquots of 475-525 μg of finely powdered carbonate material were measured into individual sample vials and loaded into the Nu Carb sample carousel. Sample digestion was achieved through the injection of ~120 μL of ~104 % H_3PO_3 at 70°C for 10 minutes, before the resulting carbon dioxide progressed into a water trap held at -95°C. CO_2 gas was then passed through a trap packed with Porapak^{TM} Q and cryogenically cooled to -34°C (Petersen *et al*., 2016). Purified CO_2 was then passed into

a cryogenically cooled "frozen finger" and total gas yield was calculated using a pressure transducer before being transferred to a sample cold finger in the mass spectrometer's dual inlet system.

Sample and reference gas were depleted at a constant rate during analysis, with active vacuum pumping performed at 150°C for 25 minutes to remove any contaminants from the adsorptive trap apparatus between each sample extraction. Measurement of purified CO_2 samples was performed by three acquisitions of sample and reference gas. 20 cycles were performed for each acquisition, with initial beam set to 80 nA and depleting to ~45 nA throughout an analytical session.

Following analysis, data was screened for unrealistic raw Δ_{47} measurements, with potentially contaminated or erroneous data removed from further analysis. Conversion into CDES and I-CDES reference frames was achieved through calibration of raw Δ_{47} measurements against measurements of ETH (distributed by S. Bernasconi from ETH Zürich) and new Carrara marble (NCM) standards (Dennis *et al*., 2011; Meckler *et al*., 2014; Bernasconi *et al*. 2018, 2021). An internal standard (P3) was also used for calibration of sample $\delta^{18}O$ and $\delta^{13}C$ measurements. 10 aliquots of carbonate material were measured for each tufa and mollusc shell sample. ETH standards were analysed in a ratio of 1:1:2 for ETH-1, ETH-2, and ETH-3, respectively, with ETH-4 excluded in favour of additional measurement of other ETH standards to increase sample Δ_{47} precision (Kocken *et al*., 2019). When converted to the CDES reference frame, ETH standard Δ_{47} values varied from accepted values by less than ± 0.010‰ for both UoA and UoM. A correction of 0.062‰ was applied after conversion to the absolute

reference frame, to project the data to an acid reaction temperature of 25 °C (Defliese et al., 2015).

Carbonate precipitation temperatures and inferred water $\delta^{18}O$ values were calculated as described in Section 3.4.

References (Appendix B)

BERNASCONI, S. M., DAËRON, M., BERGMANN, K. D., BONIFACIE, M., MECKLER, A. N., AFFEK, H. P., ANDERSON, N., BAJNAI, D., BARKAN, E., BEVERLY, E., BLAMART, D., BURGENER, L., CALMELS, D., CHADUTEAU, C., CLOG, M., DAVIDHEISER-KROLL, B., DAVIES, A., DUX, F., EILER, J., ELLIOTT, B., FETROW, A. C., FIEBIG, J., GOLDBERG, S., HERMOSO, M., HUNTINGTON, K. W., HYLAND, E., INGALLS, M., JAGGI, M., JOHN, C. M., JOST, A. B., KATZ, S., KELSON, J., KLUGE, T., KOCKEN, I. J., LASKAR, A., LEUTERT, T. J., LIANG, D., LUCARELLI, J., MACKEY, T. J., MANGENOT, X., MEINICKE, N., MODESTOU, S. E., MÜLLER, I. A., MURRAY, S., NEARY, A., PACKARD, N., PASSEY, B. H., PELLETIER, E., PETERSEN, S., PIASECKI, A., SCHAUER, A., SNELL, K. E., SWART, P. K., TRIPATI, A., UPADHYAY, D., VENNEMANN, T., WINKELSTERN, I., YARIAN, D., YOSHIDA, N., ZHANG, N. & ZIEGLER, M. (2021). InterCarb: A community effort to improve interlaboratory standardization of the carbonate clumped isotope thermometer using carbonate standards. *Geochemistry, Geophysics, Geosystems*, 22(5), e2020GC009588. https://doi.org/ 10.1029/2020GC009588

BERNASCONI, S. M., MÜLLER, I. A., BERGMANN, K. D., BREITENBACH, S. F. M., FERNANDEZ, A., HODELL, D. A., JAGGI, M., MECKLER, A. N., MILLAN, I. & ZIEGLER, M. (2018). Reducing uncertainties in carbonate clumped isotope analysis through consistent carbonate-based standardization. *Geochemistry, Geophysics, Geosystems* 19(9), 2895–2914.

BURNSIDE, N. M. (2010). U-Th dating of travertine on the Colorado Plateau: Implications for the leakage of Geologically stored CO_2. PhD thesis, University of Glasgow.

DENNIS, K. J., AFFEK, H. P., PASSEY, B. H., SCHRAG, D. P. & EILER, J. M. (2011). Defining an absolute reference frame for 'clumped' isotope studies of CO_2. *Geochimica et Cosmochimica Acta*, 75, 7117–7131. https://doi.org/10.1016/j.gca.2011.09.025

EILER, J. M. (2007). "Clumped-isotope" geochemistry – The study of naturally-occurring, multiply-substituted isotopologues. *Earth and Planetary Science Letters*, 262(3-4), 309–327. https://doi.org/10.1016/j.epsl.2007.08.020

GHOSH, P., ADKINS, J., AFFEK, H., BALTA, B., GUO, W., SCHAUBLE, E. A., SCHRAG, D. & EILER, J. M. (2006). ^{13}C–^{18}O bonds in carbonate minerals: A new kind of paleothermometer. *Geochimica et Cosmochimica Acta*, 70, 1439–1456. https://doi.org/10.1016/j.gca.2005.11.014 https://doi.org/10.1029/2017GC007385

KAUFMAN, A., BROECKER, W. S., KU, T. L. & THURBER, D. L. (1971) The status of U-series methods of mollusk dating. *Geochimica et Cosmochimica Acta*, 35(11), 1155–1183. https://doi.org/10.1016/0016-7037(71)90031-7

KOCKEN, I. J., MÜLLER, I. A. & ZIEGLER, M. (2019). Optimizing the Use of Carbonate Standards to Minimize Uncertainties in Clumped Isotope Data. *Geochemistry, Geophysics, Geosystems*, 20(11), 5565–5577. https://doi.org/10.1029/2019GC008545

MECKLER, A. N., ZIEGLER, M., MILLAN, M. I., BREITENBACH, F. M. & BERNASCONI, S. M. (2014). Long-term performance of the Kiel carbonate device with a new correction scheme for clumped isotope measurements. *Rapid Communications in Mass Spectrometry*, 28(15), 1705–1715. https://doi.org/10.1002/rcm.6949

MÜLLER, I. A., VIOLAY, M. E. S., STORCK, J.-C., FERNANDEZ, A., VAN DIJK, J., MADONNA, C. & BERNASCONI, S. M. (2017). Clumped isotope fractionation during phosphoric acid digestion of carbonates at 70 °C. *Chemical Geology*, 449, 1–14. https://doi.org/10.1016/j.chemgeo.2016.11.030

PETERSEN, S. V., WINKELSTERN, I. Z., LOHMANN, K. C. & MEYER, K. W. (2016). The effects of Porapak™ trap temperature on $\delta^{18}O$, $\delta^{13}C$, and Δ_{47} values in preparing samples for clumped isotope analysis. *Rapid Communications in Mass Spectrometry*, 30(1), 199–208. https://doi.org/10.1002/rcm.7438

APPENDIX C: XRF DATA

Table C.1: Semi-qualitative elemental abundances within sample powders for previously dated tufa samples.

Sample ID	Al	Ca[a]	Fe[a]	Mg[a]	Mn[a]	P	S	Si	Sr[a]	Ti	Zn[a]
	wt. %	wt. %	wt. %	wt. %	wt. %	wt. %	wt. %	wt. %	wt. %	wt. %	wt. %
Good Age											
DAL 1A	0.162	96.604	0.152	2.284	0.026	0.043	0.241	0.357	0.120	0.005	0.006
DAL 2A	0.166	98.187	0.052	1.061	0.009	0.022	0.108	0.330	0.053	0.006	0.006
Eliz Sp	0.131	91.225	0.041	1.582	0.021	0.066	0.018	0.835	6.059	0.017	0.005
Gosse	0.251	91.144	1.156	6.367	0.060	0.039	0.080	0.646	0.230	0.021	0.006
KEW 3	0.075	98.952	0.114	0.572	0.026	0.048	0.065	0.091	0.048	0.005	0.004
SUL 1a[b]	0.231	95.116	0.059	0.560	0.040	0.049	0.105	0.745	3.004	0.085	0.005
SUL 1b[b]	0.225	95.304	0.057	0.447	0.030	0.043	0.110	0.691	3.049	0.035	0.009
SUL 1c[b]	0.161	95.833	0.050	0.000	0.012	0.038	0.064	0.632	3.184	0.022	0.005
SUL 1d[b]	0.392	94.392	0.115	0.601	0.014	0.046	0.065	1.056	3.266	0.043	0.009
SUL 1e[b]	0.267	93.817	0.089	0.779	0.032	0.059	0.060	1.073	3.775	0.044	0.004
SUL 1f[b]	0.131	95.395	0.026	0.287	0.046	0.059	0.050	0.565	3.421	0.016	0.006
WAR 1	0.316	91.374	2.128	3.718	0.053	0.021	0.728	1.193	0.441	0.023	0.005
WAR 5	0.177	92.606	4.394	1.791	0.163	0.038	0.087	0.634	0.090	0.013	0.006
WAR 7	0.247	97.243	0.409	1.244	0.030	0.023	0.187	0.500	0.101	0.013	0.004
Poor Age											
BER 2	0.056	69.101	0.603	28.282	0.020	0.015	0.098	0.606	1.211	0.007	0.001
BLAN A	0.209	86.624	0.544	9.726	0.021	0.017	0.163	2.021	0.650	0.021	0.003
DAL A	0.115	97.754	0.103	1.409	0.059	0.036	0.102	0.343	0.071	0.003	0.004
DAL 5	0.231	95.818	0.342	1.886	0.055	0.021	0.164	1.382	0.086	0.012	0.004
ELIZ A	0.022	68.287	0.048	30.154	0.000	0.027	0.033	0.414	1.009	0.004	0.001
ELIZ Ca	0.057	80.967	0.017	17.898	0.009	0.030	0.073	0.180	0.759	0.008	0.003
ELIZ Cb	0.054	53.611	0.033	45.041	0.000	0.025	0.081	0.229	0.914	0.011	0.000
ELIZ D	0.054	94.823	0.036	0.000	0.008	0.068	0.019	0.481	4.501	0.009	0.002
JER 3	0.090	61.039	0.064	37.041	0.014	0.033	0.082	0.703	0.917	0.014	0.002
WAR 7a	0.118	98.044	0.024	1.177	0.010	0.025	0.109	0.184	0.301	0.002	0.006
WAR 7b	0.062	93.827	0.011	5.243	0.010	0.025	0.214	0.149	0.454	0.002	0.003

[a]assumed to be part of XCO_3 compounds
[b]samples used for clumped isotope analysis

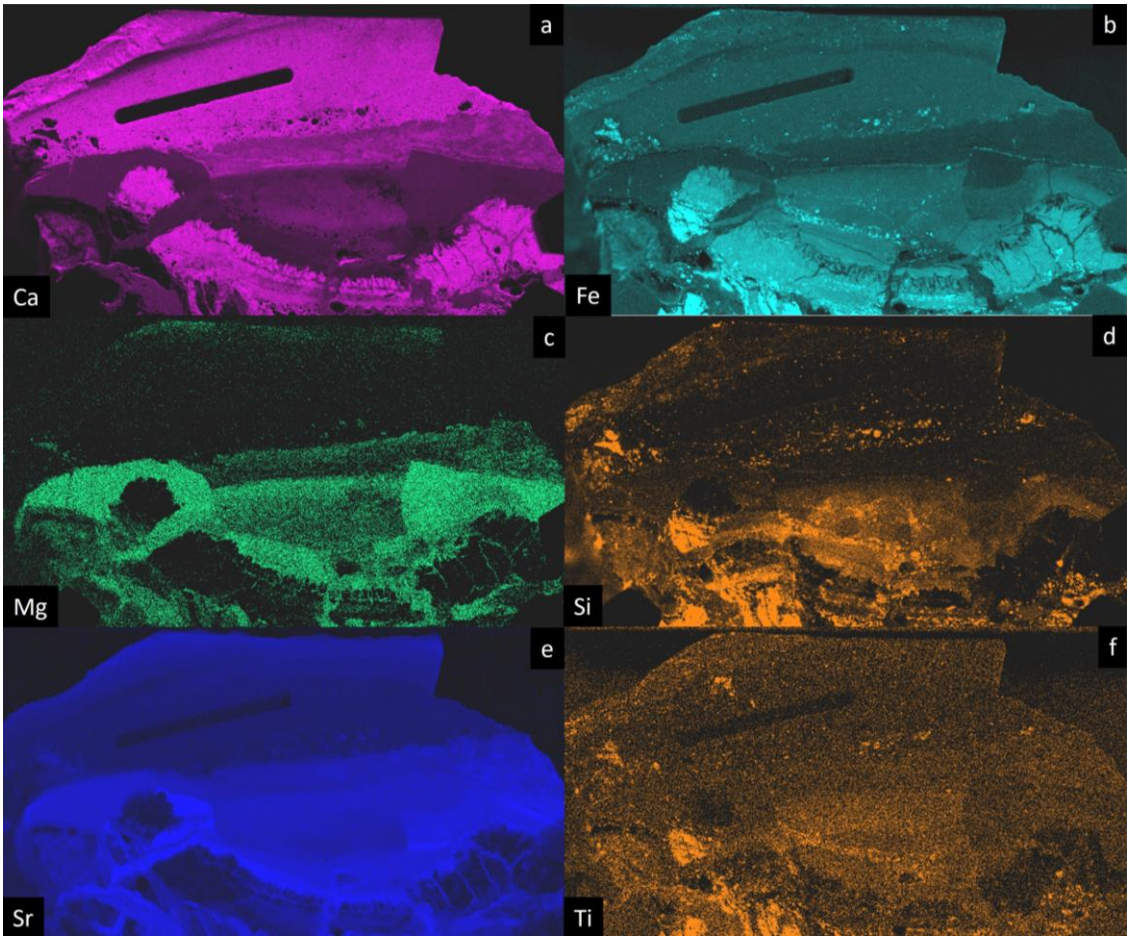

Figure C.1: XRF map for the well dated single tufa sample from Gosse Spring, showing relative abundances for a) calcium; b) iron; c) magnesium; d) silicon; e) strontium; and f) titanium. At least three mineral phases can be identified, with the dated calcite layer more calcium-rich than the magnesium and strontium-enriched phase. Material enriched in silicon and iron likely represents detrital material in the tufa sample. The Mg-Sr phase has not been dated or undergone XRD analysis, although it is likely a secondarily deposited dolomitic phase, which is supported by infilling of the lower calcium-rich phase.

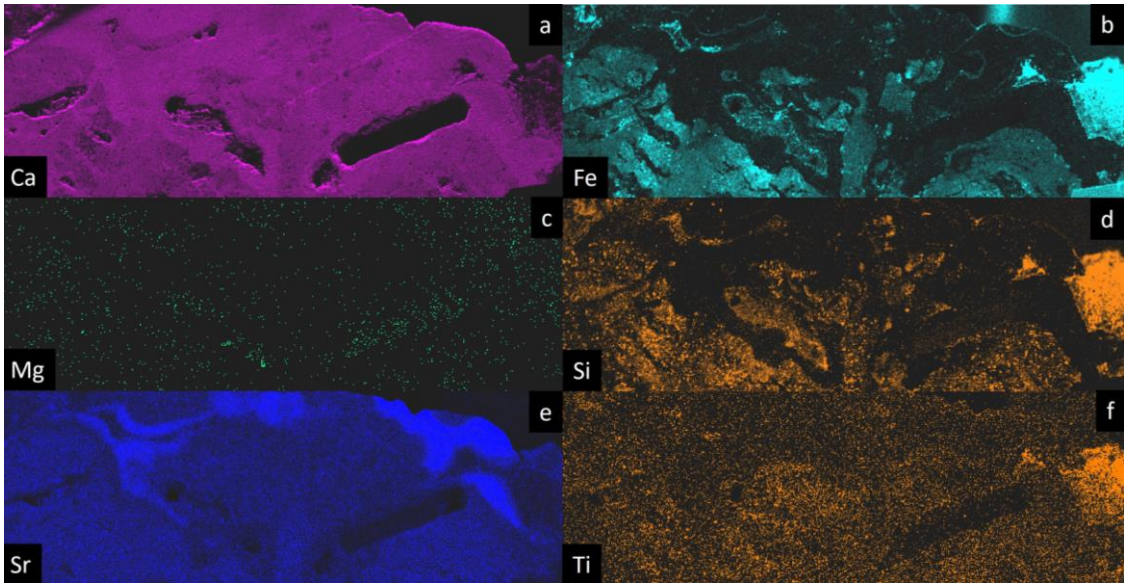

Figure C.2: XRF map for the well dated DAL 2A tufa sample from Dalhousie Springs, showing relative abundances for a) calcium; b) iron; c) magnesium; d) silicon; e) strontium; and f) titanium. Detrital material in the sample can be identified by enriched silicon and iron, along with a slight decrease in calcium abundance. Enriched strontium zones may represent changes in spring water composition.

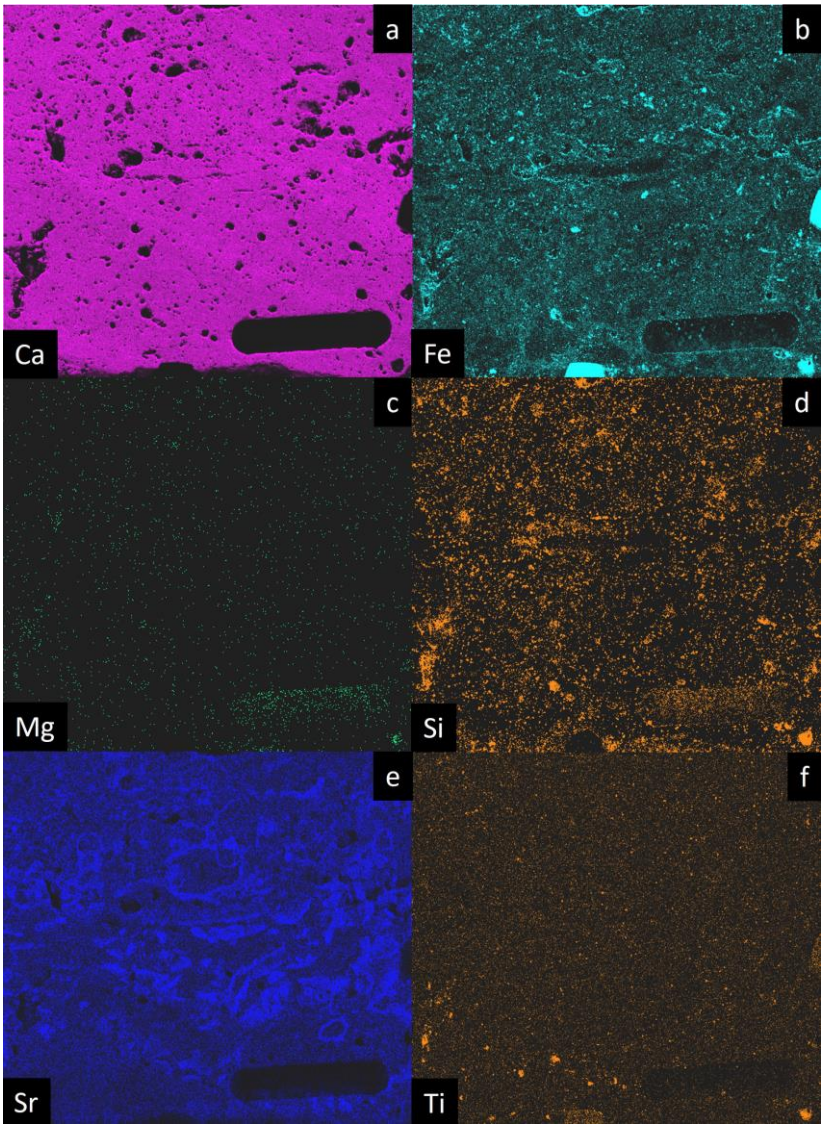

Figure C.3: XRF map for the poorly dated DAL A tufa sample from Dalhousie Springs, showing relative abundances for a) calcium; b) iron; c) magnesium; d) silicon; e) strontium; and f) titanium. XRD analysis for the sampled layer indicated a composition of only calcite and quartz. Areas with enriched silicon and low calcium are likely indicative of changes in height (void spaces) in the sample, rather than lithic fragments. Enriched strontium zones may represent secondarily precipitated carbonate.

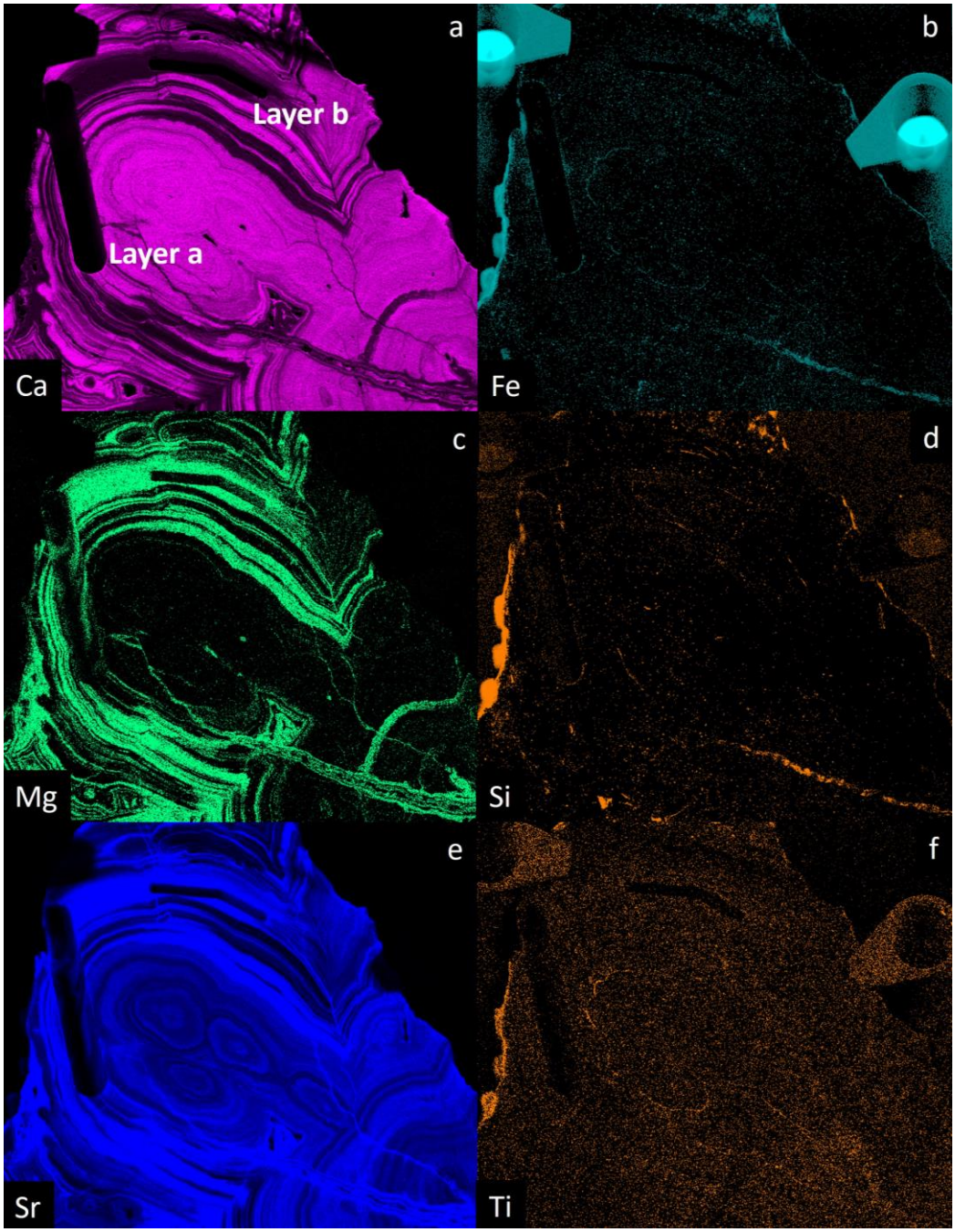

Figure C.4: XRF map for the poorly dated ELIZ C tufa sample from Elizabeth Springs, showing relative abundances for a) calcium abundance with layers a and b labelled for reference; b) iron; c) magnesium; d) silicon; e) strontium; and f) titanium. XRD analysis for Layer a indicated the presence of calcite and dolomite. Layers of dolomite can be seen amongst calcite layers, as best shown by the calcium and magnesium XRF maps, with dolomite (high Mg) veins also seen cutting across the carbonate.

Non-metric multidimensional scaling (NMDS) was applied to assess how elemental compositions vary with respect to U-series dating quality (Figure C.5). NMDS effectively condenses multidimensional data into two dimensions to enable visualisation and interpretation (Faith *et al*., 1987; Minchin, 1987). As with PCA (Section 4.1), NMDS is able to distinguish dolomite-bearing poorly-dated tufa samples, but is unable to differentiate poorly-dated tufas for which dolomite is absent.

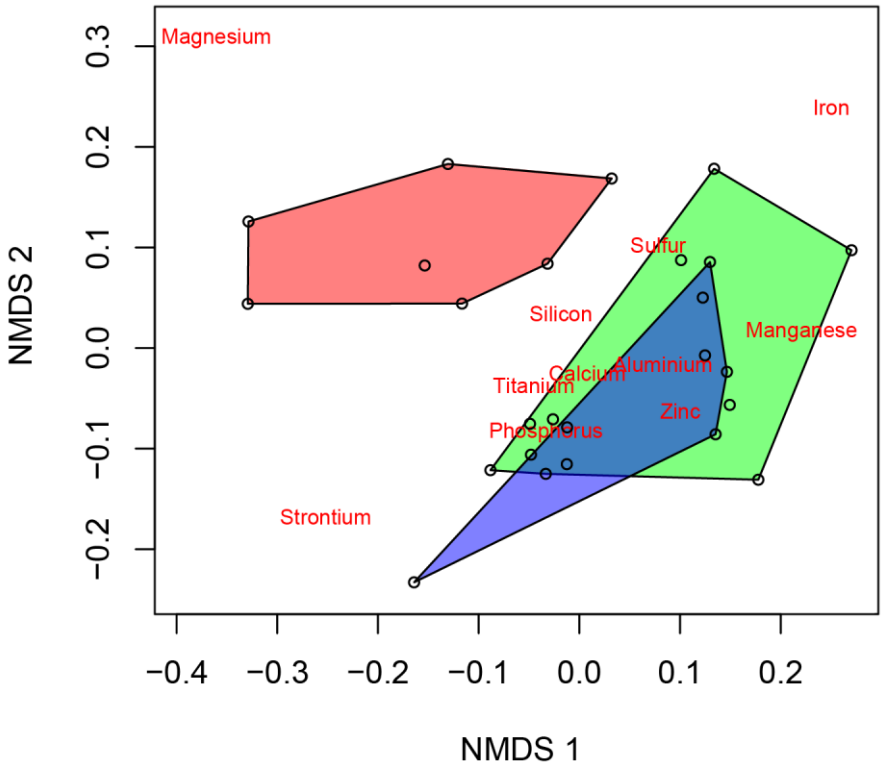

Figure C.5: Non-metric multidimensional scaling analysis for XRF data from central Australian mound spring tufas. Well-dated tufas are indicated by the green shading, with poorly-dated tufa samples separated in dolomite-bearing (red) and dolomite-absent (blue) subgroups.

APPENDIX D: ADDITIONAL ISOTOPE DATA

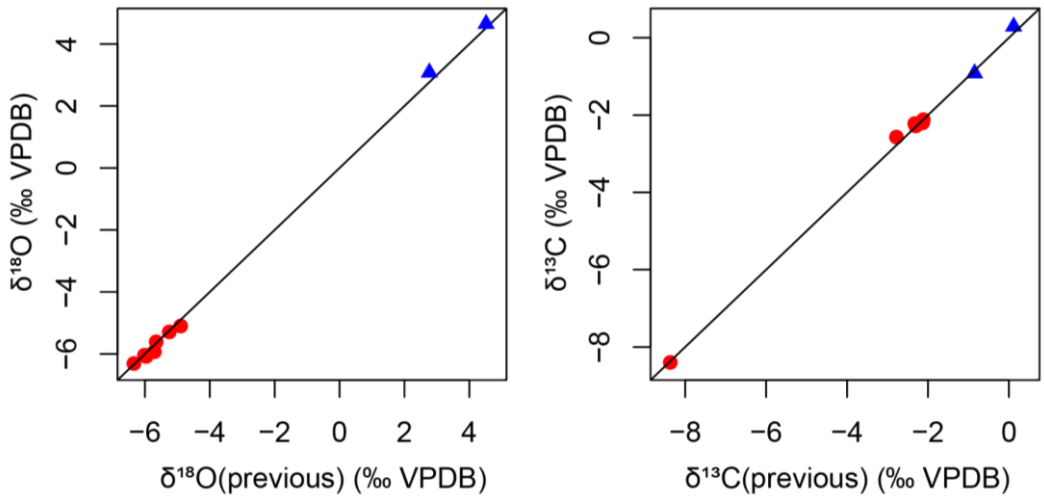

Figure D.1: Comparison of tufa and lake shell $\delta^{18}O$ and $\delta^{13}C$ values, relative to previous analyses by for tufas and lake shells (Cohen *et al*., in prep.). Tufa samples are shown as red circles, while lake shells are shown as blue triangles. The black 1:1 line is included for reference.